Petroleum Science 23 (2026) 7052–7071

Contents lists available at ScienceDirect

Petroleum Science

journal homepage: www.keaipublishing.com/en/journals/petroleum-science

Original Paper

Investigating the impact of well data and seismic resolution on porosity prediction using Bayesian deep learning

Guo-Yin Zhang [a,b,c,*], Quan Xiong [a,b,c], Xin Zhang [a,b,c], Wen-Qi Yang [a,b,c], Yu-Qing He [a,b,c], Xin-Xin Wang [d], Kong-Hang Yang [d], Cheng-Yan Lin [a,b,c]

[a] National Key Laboratory of Deep Oil and Gas, China University of Petroleum (East China), Qingdao, 266580, Shandong, China
[b] School of Geosciences, China University of Petroleum (East China), Qingdao, 266580, Shandong, China
[c] Shandong Provincial Key Laboratory of Reservoir Geology, China University of Petroleum (East China), Qingdao, 266580, Shandong, China
[d] Tarim Oilfield Company, PetroChina, Korla, 841000, Xinjiang, China

ARTICLE INFO

Article history:
Received 28 December 2025
Received in revised form
4 March 2026
Accepted 29 April 2026
Available online 4 May 2026

Edited by Jie Hao

Keywords:
Bayesian deep learning
Uncertainty
Well quantity
Seismic resolution
Continuous wavelet transform

ABSTRACT

Seismic porosity inversion is inherently ill-posed and highly sensitive to seismic resolution, geological complexity, and well density, particularly in thin-bedded heterogeneous reservoirs. Although deep-learning-based inversion has shown promising results, most approaches remain deterministic and lack reliable uncertainty quantification. In this study, we examine the combined effects of input representation, Bayesian inference, well density, and seismic resolution on porosity inversion using Bayesian deep learning. Two encoder–decoder networks are developed: WaveNet (waveform-based) and SpecNet (time–frequency spectral-based). Their Bayesian versions, BayeWaveNet and BayeSpecNet, incorporate Monte Carlo dropout for uncertainty estimation. A series of controlled experiments is conducted on a synthetic fluvial–deltaic reservoir model under varying seismic frequencies (20–60 Hz) and well densities, and field seismic data are further used to validate the conclusions. Results show that spectral inputs outperform waveform inputs, especially for thin-bedded channels and deltaic deposits. Bayesian models yield more stable, geologically consistent predictions with reduced noise and meaningful uncertainty estimates. Increasing well density and seismic frequency significantly improves accuracy and reduces uncertainty. Overall, BayeSpecNet achieves the best performance, demonstrating the value of integrating spectral representations and Bayesian learning for reliable, risk-aware reservoir characterization.

© 2026 The Authors. Publishing services by Elsevier B.V. on behalf of KeAi Communications Co. Ltd. This is an open access article under the CC BY license (http://creativecommons.org/licenses/by/4.0/).

1. Introduction

Seismic inversion remains a key tool for quantitative subsurface characterization, aiming to estimate reservoir properties such as impedance and porosity from seismic data. Despite continuous methodological advances, seismic inversion is inherently ill-posed and sensitive to data quality, prior assumptions, and geological complexity. These challenges are particularly pronounced in environments with thin-bedded deposits, strong lateral heterogeneity, sparse well control, and limited seismic resolution (Zeng and Hentz, 2004; Zhang et al., 2018).

Data-driven seismic inversion based on deep learning has attracted increasing attention as an alternative to conventional physics-based approaches (Song et al., 2022; Su et al., 2023; Zhang et al., 2018, 2025b; Zhao et al., 2021). By learning nonlinear mappings directly from seismic data to reservoir properties, deep neural networks have demonstrated improved prediction accuracy and computational efficiency (Dong et al., 2022; Li et al., 2025; Tao et al., 2025; Zhang et al., 2025b). Convolutional neural networks, Encoder–decoder, U-net, Recurrent neural networks, Bidirectional Long Short-Term Memory, and Transformer architectures have been successfully applied to impedance and porosity inversion using seismic waveforms (Das et al., 2019; Sun et al., 2024; Xu et al., 2024; Zhang et al., 2022b).

To further improve the performance of deep-learning-based seismic inversion, various strategies have been proposed, including network architecture design, input representation enhancement, and uncertainty-aware learning (Zhang et al., 2024;

* Corresponding author.
E-mail address: zhanggy@upc.edu.cn (G.-Y. Zhang).
Peer review under the responsibility of China University of Petroleum (Beijing).

https://doi.org/10.1016/j.petsci.2026.04.050
1995-8226/© 2026 The Authors. Publishing services by Elsevier B.V. on behalf of KeAi Communications Co. Ltd. This is an open access article under the CC BY license (http://creativecommons.org/licenses/by/4.0/).

Zhang and Yang, 2025; Zhao et al., 2025). Zhang et al. (2018) introduced time–frequency representations as network inputs to better exploit spectral and multiscale information embedded in seismic signal, and highlighted the advantage of spectral information in enhancing thin-bed prediction. Recent research also proves that the time–frequency spectrum improves sensitivity of deep learning models to stratigraphic variations and thin-bed responses compared with waveform-only approaches (Manzoor et al., 2024; Zhang et al., 2020, 2025a).

Uncertainties are inherent in seismic interpretation and inversion, and uncertainty quantification has long remained a challenging problem (Bosch et al., 2010; Grana et al., 2022; Pradhan and Mukerji, 2020; Thore, 2015). However, most existing deep-learning-based inversion methods remain deterministic and provide only single best-estimate predictions. As a result, they fail to explicitly quantify uncertainty arising from limited training data, band-limited seismic resolution, and model non-uniqueness. In real-field applications, limited well availability significantly reduces the representativeness of training samples, while restricted seismic bandwidth further degrades the resolution of thin layers and subtle geological features. These factors jointly increase prediction uncertainty and reduce the reliability of inversion results, highlighting the necessity of uncertainty-aware data-driven inversion frameworks (Schaaf and Bond, 2019).

Recent advances in Bayesian deep learning offer a promising solution by integrating probabilistic inference into neural networks, enabling simultaneous prediction and uncertainty estimation (Choi et al., 2020; Li et al., 2024; Mukhopadhyay and Mallick, 2019; Zhang et al., 2022a). Bayesian neural networks and variational inference techniques allow predictive uncertainty to reflect data coverage, seismic resolution, and geological complexity. Nevertheless, systematic investigations that jointly examine input representation (waveform vs. time–frequency spectrum), Bayesian vs. non-Bayesian learning, and training data scenarios (well density and seismic resolution) remain limited in the context of seismic inversion.

To address these challenges, we propose two Bayesian deep-learning–based seismic inversion frameworks, namely BayeWaveNet and BayeSpecNet, and systematically investigate the effects of well data availability and seismic resolution on porosity inversion performance using Bayesian deep learning through a series of contrastive inversion experiments. BayeWaveNet operates directly on seismic waveforms, and BayeSpecNet exploits time–frequency spectral representations to capture multiscale seismic information. Through comprehensive experiments incorporating waveform- and spectrum-based inputs, Bayesian versus non-Bayesian frameworks, different well densities, and varying seismic frequency contents, we demonstrate that Bayesian spectral-domain inversion yields superior accuracy and stability, together with physically meaningful uncertainty estimates that are consistent with data availability and seismic resolution.

2. Network architecture for seismic inversion

Neural networks with different architectures are designed according to the characteristics of seismic waveforms and porosity data. Inspired by SegNet proposed by Badrinarayanan et al. (2017), we develop two encoder–decoder frameworks, WaveNet and SpecNet, for seismic inversion (Fig. 1). Both models adopt a convolutional encoder–decoder architecture, but differ in input dimensions and convolutional configurations (Table 1).

(1) WaveNet

WaveNet comprises an encoder and a decoder (Fig. 1). The encoder extracts high-dimensional representations from the input seismic data, while the decoder reconstructs the corresponding porosity predictions from these latent features.

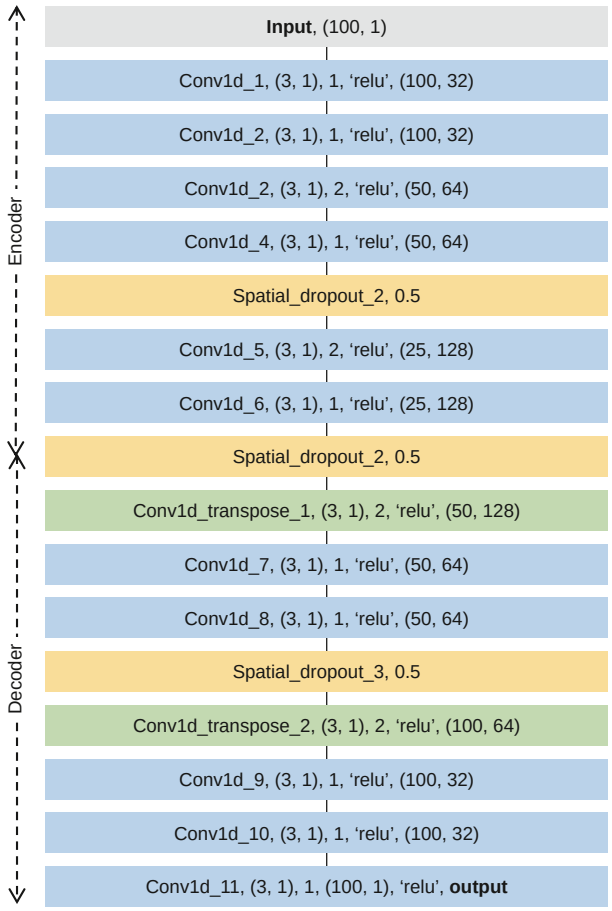


Fig. 1. Architecture of the WaveNet model. The network accepts input tensors of size (100, 1). The convolution layers are marked as blue boxes, with annotated parameters including layer name, kernel size, stride length, activation function, and output feature dimensions. The final convolution layer acts as the output layer. Spatial dropout layers are marked as orange boxes, and the dropout rate is assigned the value of 0.5. Transposed convolution layers are marked as green boxes.

The convolution operation in each layer is formulated as:

$$\boldsymbol{q}_j = f\left(\sum_{i=1}^{I} \boldsymbol{o}_i * \boldsymbol{w}_{i,j}\right),\ j = 1, 2, \ldots, J \tag{1}$$

where $\boldsymbol{o}_i$ denotes the i-th input seismic trace, $\boldsymbol{q}_j$ represents the j-th output feature map, * indicates the convolution operation, and $\boldsymbol{w}_{i,j}$ is the convolution kernel connecting $\boldsymbol{o}_i$ and $\boldsymbol{q}_j$. Here, I is the number of input channels and J is the number of output feature maps (kernels). The function f denotes the nonlinear activation.

The input to WaveNet is the original seismic waveform with a size of (100, 1). One-dimensional convolutional kernels of size (3, 1) are used. The stride is set to 1 or 2. In the encoder, convolutional layers with stride 2 progressively reduce the feature map size while increasing the number of kernels, enabling extraction of higher-level abstract features. In the decoder, transposed convolutional layers with stride 2 are applied to upsample the feature maps and gradually recover the original resolution. Thus, the feature map size decreases in the encoder and increases symmetrically in the decoder. ReLU is adopted as the activation function for both convolutional and transposed convolutional layers (Nair and Hinton, 2010). Spatial Dropout is introduced for

Table 1
Different network architectures for seismic inversion.

Name	Input, size	Size of the first-layer convolution kernels	Trainable parameters	Dropout turns on in prediction mode	Results
WaveNet	Waveform, (100,1)	(3,1)	157,537	No	Porosity
SpecNet	Spectrum, (100,19)	(3,19)	159,265	No	Porosity
BayeWaveNet	Waveform, (100,1)	(3,1)	157,537	Yes	Porosity and uncertainty
BayeSpecNet	Spectrum, (100,19)	(3,19)	159,265	Yes	Porosity and uncertainty

regularization to mitigate overfitting (Srivastava et al., 2014). During training, Dropout randomly deactivates a fraction of neurons at each iteration, while the remaining activations are scaled by 1/(1-rate) to maintain the expected output magnitude. The training of WaveNet involves optimizing the learnable convolutional kernels using a loss function and an optimizer. The mean squared error (MSE) is employed as the loss function, and the adaptive moment estimation (Adam) algorithm is used for parameter optimization (Kingma and Ba, 2014). The initial learning rate is set to 0.001.

(2) SpecNet

SpecNet adopts a network architecture similar to that of WaveNet, but differs in the form of input data. Instead of raw seismic waveforms, SpecNet takes time–frequency transformed spectra as input. The time-frequency spectrum was obtained using continuous wavelet transform, with a decomposition frequency range of 10–100 Hz and a frequency interval of 5 Hz. The input spectrum has a size of (100, 19), and accordingly, the kernel size of the first convolutional layer is set to (3, 19) to integrate information across the full spectral dimension. Subsequent layers employ similar 1D convolutional operations and hyperparameter settings as those in WaveNet, ensuring comparable network depth and model capacity. Although 2D convolutional layers were used for seismic inversion in our previous study (Zhang et al., 2018), we adopt 1D convolutional layers in this work. This design choice allows the model to focus on vertical trace-wise feature extraction, reduces computational complexity, and facilitates a clearer comparison between waveform-based and spectral-domain inversion frameworks. At the initial experimental design stage, we also considered the potential advantages of 2D convolutions over 1D convolutions for feature extraction. However, comparative experiments demonstrated that inversion networks utilizing 1D convolution layers exhibit performance comparable to their 2D counterparts, while also offering significantly reduced computational costs during model training. We therefore adopted 1D convolutions in the final network.

(3) BayeWaveNet and BayeSpecNet

BayeWaveNet and BayeSpecNet extend WaveNet and SpecNet by incorporating Bayesian deep learning to enable uncertainty quantification. Conventional deep learning models learn deterministic network parameters, whereas Bayesian deep learning infers distributions over the network weights, thereby allowing predictive uncertainty to be explicitly characterized.

Dropout provides an efficient approximation to Bayesian inference in neural networks (Gal and Ghahramani, 2016; Kendall and Gal, 2017). Originally introduced as a regularization technique to mitigate overfitting (Srivastava et al., 2014), dropout randomly deactivates a subset of feature units during training. In standard deep learning, dropout is applied only during training; in contrast, Bayesian deep learning retains dropout during both training and inference, enabling Monte Carlo (MC) sampling from an approximate posterior distribution over the weights.

For a given input–output pair $\{\boldsymbol{x}^*, \boldsymbol{y}^*\}$, each stochastic forward pass with dropout produces a prediction $\widehat{\boldsymbol{y}}^*$ that can be regarded as a Monte Carlo sample from the approximate posterior $q(\boldsymbol{W})$. After performing T stochastic forward passes, the predictive mean and standard deviation are estimated as:

$$\mathbb{E}(\boldsymbol{y}^*) = \frac{1}{T}\sum_{t=1}^{T}\widehat{\boldsymbol{y}}^*(\boldsymbol{x}^*, \boldsymbol{W}_t), \tag{2}$$

$$\sigma(\boldsymbol{y}^*) = \sqrt{\frac{1}{T}\sum_{t=1}^{T}(\mathbb{E}(\boldsymbol{y}^*) - \widehat{\boldsymbol{y}}^*(\boldsymbol{x}^*, \boldsymbol{W}_t))^2}, \tag{3}$$

where $\boldsymbol{W}_t \sim q(\boldsymbol{W})$ denotes the t-th weight sample from the approximate posterior. Each stochastic prediction thus represents one MC sample of the predictive distribution. A dropout rate of 0.5 is applied to three designated layers, randomly deactivating 50% of the feature units during each training and inference pass (Fig. 1). The training procedure for the Bayesian models follows the same framework as the non-Bayesian counterparts (WaveNet and SpecNet), employing mean squared error (MSE) as the loss function and the Adam optimizer for parameter updating.

Bayesian deep learning offers two key advantages over conventional approaches.

- Uncertainty quantification: Provides probabilistic outputs with inherent uncertainty estimates
- Enhanced robustness: Demonstrates greater stability against weight perturbations compared to non-Bayesian models

The Bayesian deep learning method directly provides quantitative uncertainty estimates for each prediction, with the core mechanism being Monte Carlo Dropout (MCDO). MCDO interprets the random activation and deactivation of neurons in the Dropout layer as a sampling process of the posterior weight distribution of the trained model within the Bayesian framework, enabling approximate inference of the posterior distribution without resorting to complex Bayesian computational procedures (Gal and Ghahramani, 2016). Uncertainty is generated inherently and synchronously during the inference phase. For each input sample, we perform a specified number of stochastic forward propagation rounds with the Dropout layer activated. The standard deviation of the resulting predictions from these multiple rounds is defined as the quantitative uncertainty estimate for the corresponding prediction point, while the mean value yields the final predicted result.

While traditional deep learning models may exhibit high sensitivity to minor weight variations, Bayesian approaches mitigate this through Monte Carlo sampling during inference. This repeated sampling averages out the effects of individual weight changes, though at increased computational cost. The

computational overhead remains manageable through GPU parallelization, with individual predictions completing in seconds.

(4) Model training and deploying

The four inversion networks proposed earlier exhibit distinct characteristics in terms of both input data and network architecture. Table 1 summarizes the key architectural specifications and capabilities of four deep learning models developed for seismic inversion. The framework compares two baseline architectures (WaveNet and SpecNet) with their Bayesian counterparts (BayeWaveNet and BayeSpecNet). WaveNet processes 1D waveform inputs of size (100,1) using first-layer convolutional kernels of size (3,1), containing 157,537 trainable parameters, while SpecNet operates on 2D spectral inputs (100,19) with correspondingly wider kernels (3,19), yielding 159,265 parameters. The Bayesian variants maintain identical architectures to their standard counterparts but activate dropout during prediction to enable uncertainty quantification. All models predict porosity, with the Bayesian versions additionally providing uncertainty estimates through Monte Carlo dropout sampling. This systematic comparison highlights the architectural trade-offs between computational complexity (parameter count) and probabilistic functionality.

Considering practical applications, all models are trained using well logs and adjacent seismic traces. Following training, the deep learning models are deployed to perform predictions on the entire 3D seismic volume. This enables the generation of spatially continuous porosity estimates and associated uncertainty quantification. Fig. 2 illustrates the integrated workflow for porosity prediction from 3D seismic data using deep learning. The process begins with input data preparation, comprising: (1) waveform samples and time-frequency spectra extracted from near-well seismic traces, and (2) corresponding porosity measurements from well logs. These data pairs are used to train four distinct neural network architectures: standard WaveNet and SpecNet models process waveform and spectral inputs respectively, while their Bayesian counterparts (B-WaveNet and B-SpecNet) additionally quantify prediction uncertainty through Monte Carlo dropout. During deployment, raw seismic data undergoes the same feature extraction to generate network inputs. The system outputs both porosity predictions and associated uncertainty estimates, enabling probabilistic interpretation of reservoir properties. This end-to-end framework bridges seismic measurements with petrophysical characterization while providing crucial uncertainty quantification for risk assessment.

3. Synthetic dataset

A synthetic dataset was constructed to evaluate the performance of the proposed methods under diverse geological scenarios. Based on the publicly available Stanford VI reservoir model, the dataset was designed to simulate realistic reservoir properties and spatial heterogeneity.

The Stanford VI model consists of 150 × 200 × 200 grid cells in the *x*, *y*, and *z* directions, respectively. The horizontal resolution is 25 m in both *x* and *y* directions, and the vertical resolution is 1 m. This high-resolution framework enables the generation of geologically consistent synthetic seismic and well data, providing a robust benchmark for validating the Bayesian deep-learning–based porosity inversion approach.

The geological model represents a fluvial depositional system that defines the facies framework of the reservoir. From bottom to top, deltaic deposits, meandering channels, and sinuous channels are sequentially developed. Porosity is simulated independently for each facies using the sequential Gaussian simulation algorithm (Fig. 3a). Porosity stochastic simulation was controlled by facies. The porosity distributions and variogram parameters for different facies are documented in Castro et al. (2005). Elastic properties—including density, P-wave velocity, and acoustic impedance—are subsequently derived from the simulated facies and porosity values, based on established laboratory relationships and theoretical formulas. For further details regarding the methods and parameters employed in the geological and petrophysical modeling processes, please refer to Lee and Mukerji (2012) and Castro et al. (2005).

The synthetic seismic data are generated as zero-offset responses from the acoustic impedance model using the acoustic impedance model using Ricker wavelets with varying central frequencies and the same maximum amplitude. Fig. 3 displays the synthetic zero-offset seismic data at 20, 40, and 60 Hz. Both the wavelets and seismic data are converted from time domain to

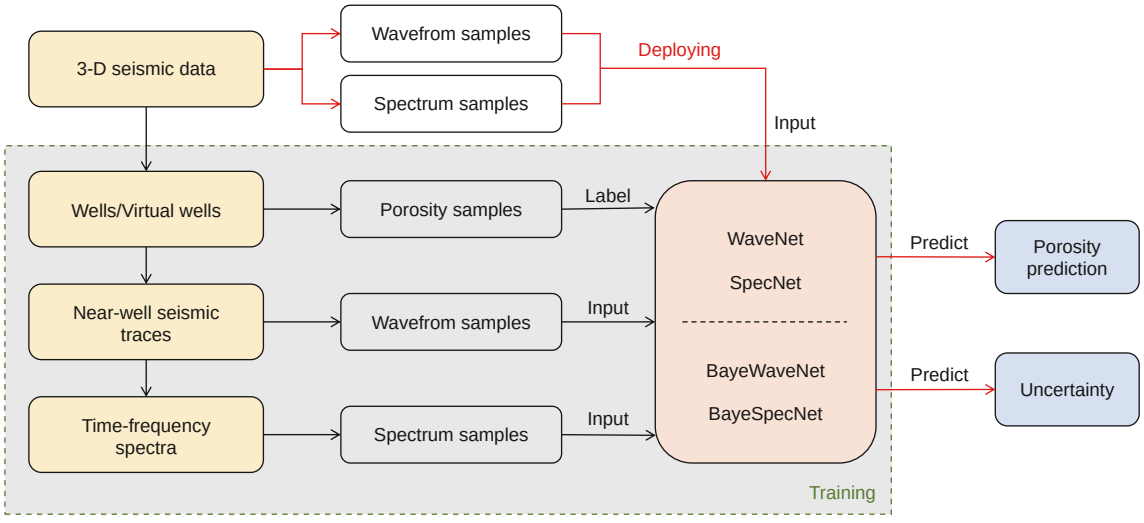


Fig. 2. Workflow of model training and deploying. The green dotted box denotes the model training workflow, while the red flow connections denote the model deploying workflow.

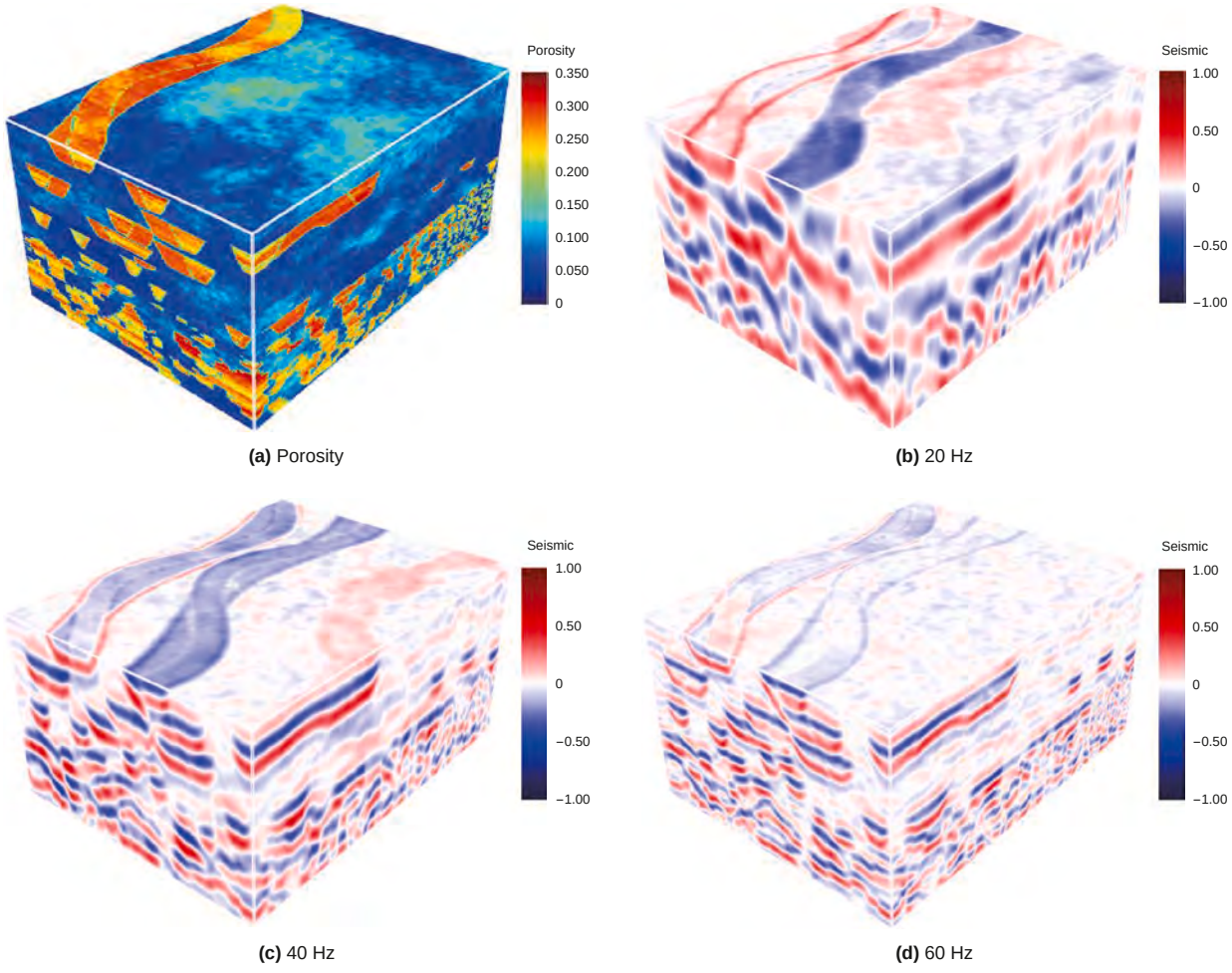


Fig. 3. 3D porosity and synthetic seismic data. **(a)** 3D porosity data. **(b)** 3D synthetic seismic data of 20 Hz. **(c)** 3D synthetic seismic data of 40 Hz. **(d)** 3D synthetic seismic data of 60 Hz.

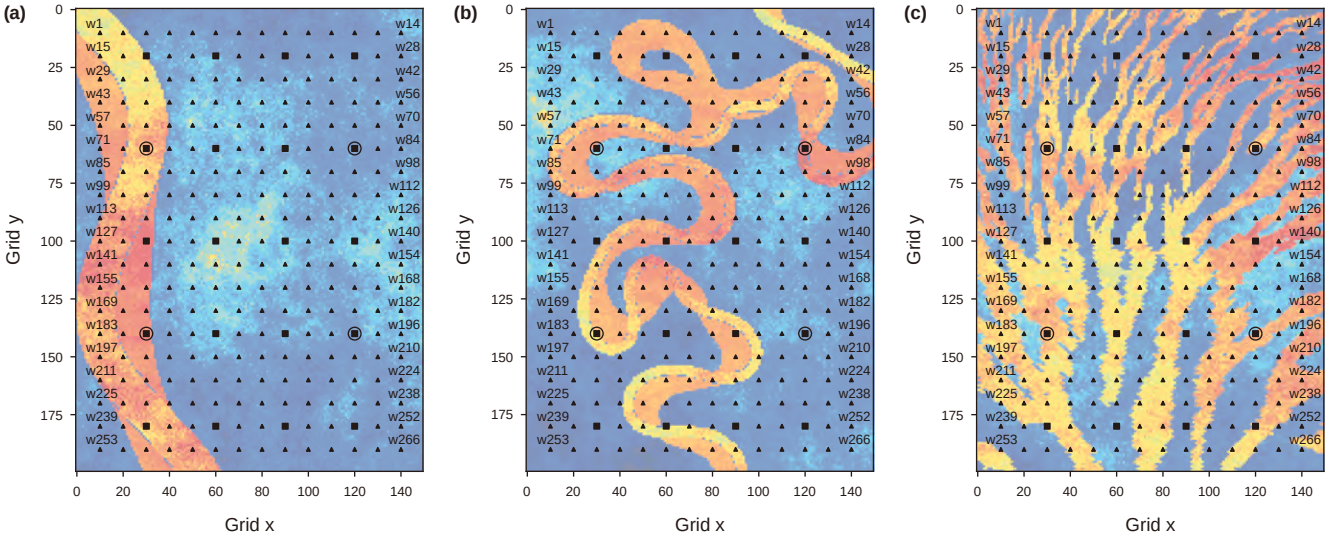


Fig. 4. Locations of the 266 virtual wells uniformly distributed across horizontal slices representative of different sedimentary facies. **(a)** Sinuous channel facies at Grid 0; **(b)** Meandering channel facies at Grid 80; **(c)** Deltaic deposits at Grid 120. Among these, four wells (marked with circles) and twenty wells (marked with squares) are selected to simulate scenarios with sparse and moderate well availability, respectively.

depth domain using the corresponding velocity model to ensure spatial alignment with the porosity model. These depth-aligned seismic and porosity volumes are employed as input features and label data, respectively, for training the deep learning models.

To enhance the realism of porosity prediction, synthetic virtual wells were generated for this study. A total of 266 virtual wells were designed, as illustrated in Fig. 4. From these locations, both porosity logs and their corresponding nearby seismic traces were extracted to construct the training dataset for the deep learning models. To maintain clarity in both the training dataset and the subsequent comparative experiment design, only one nearby seismic trace per well is employed. Fig. 5a presents a porosity cross-section, overlaid with the virtual well positions and their corresponding extracted porosity logs. These porosity logs were used as label data and paired with the surrounding seismic traces (Fig. 5b), thereby establishing a rigorous supervised learning framework for seismic porosity inversion.

The inclusion of multiple facies with distinct sedimentary characteristics enables a comprehensive evaluation of the robustness of the deep learning models across varying geological settings (Fig. 4). Three facies types, sinuous channels, meandering channels, and deltaic deposits, were simulated within depth intervals, 0-79, 80-119, and 120-199, respectively, along the *z*-direction (Fig. 5a). Sinuous channels are characterized by high sinuosity and greater sand thickness, typically ranging between 15 m and 20 m. In contrast, meandering channels exhibit even higher sinuosity but are thinner, with thicknesses varying from approximately 5 m to 10 m. Deltaic deposits demonstrate pronounced lateral heterogeneity in the *y*-direction, showing a gradual decrease in both thickness and width from one side to the

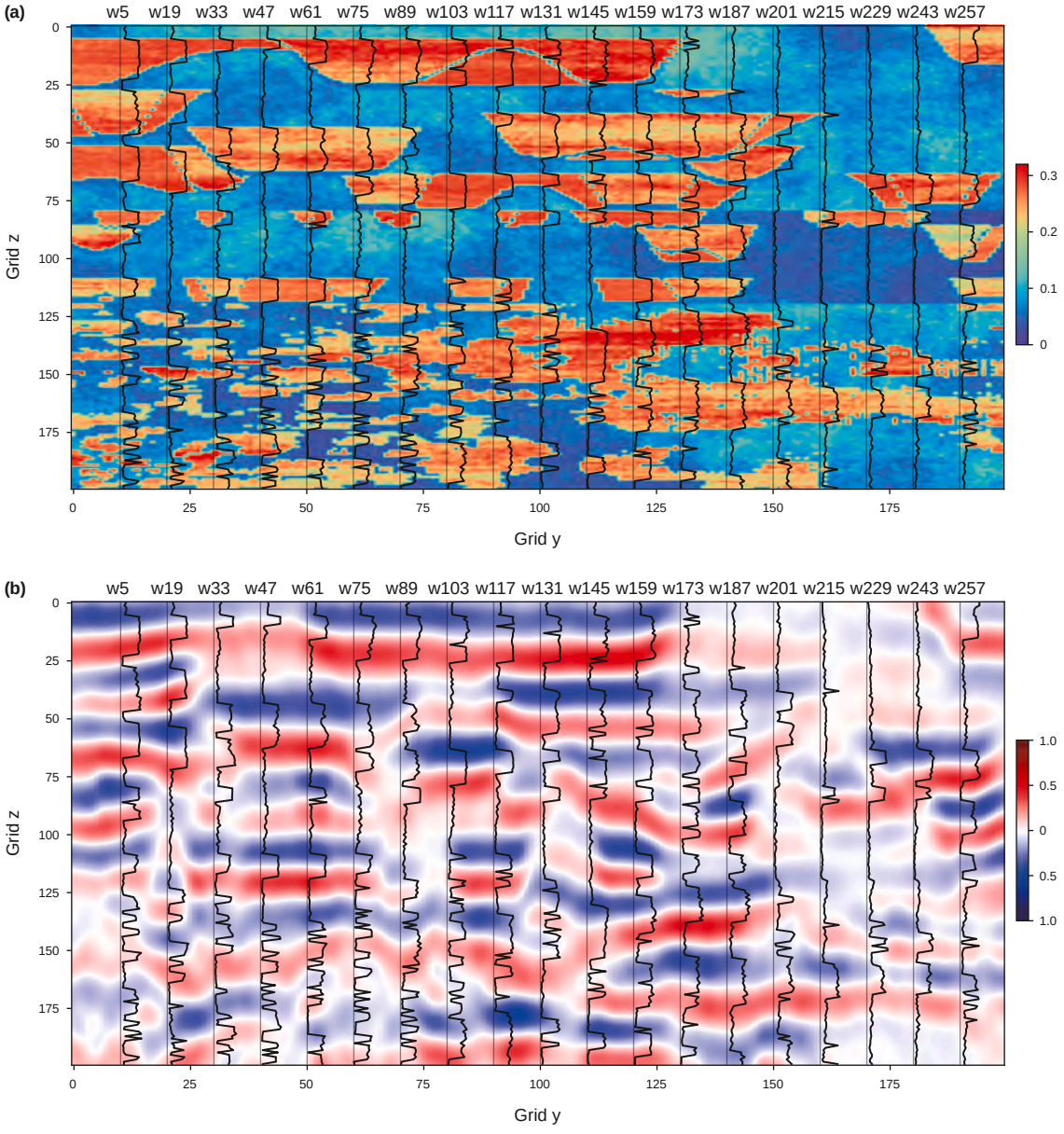


Fig. 5. Cross-sections of seismic and porosity data along grid line $x = 50$ with virtual well locations. **(a)** Porosity section showing virtual wells and their corresponding extracted porosity logs. **(b)** Seismic section (40 Hz) displaying the same set of virtual wells with associated porosity logs. The porosity logs from these wells serve as training labels, while the adjacent seismic traces function as input features for the deep learning models.

Table 2
Data scenarios for deep learning model training.

Scenario number	Description	Number of wells	Seismic frequencies, Hz
1	Sparse or limited well condition	4	20, 30, 40, 50, 60
2	Moderate well condition	20	
3	Dense well condition	266	

other (Figs. 4c and 5a). Their thickness varies significantly across the model, ranging from about 1 m to 25 m.

In practical applications, the availability of well data often varies significantly, influenced by factors such as reservoir type and the stage of reservoir development. In order to evaluate the performance of the deep learning models under varying data availability conditions, different numbers of wells are selected as training data in different scenarios (Table 2). The training datasets consisting of 4, 20, and 266 wells simulate real-world situations with sparse, moderate, and dense well conditions, respectively. Well location selection can affect the representativeness of training samples to some extent, thereby influencing model training and prediction performance, especially under sparse well conditions. For the 4-well scenario, we selected well locations to ensure a relatively uniform distribution and avoid clustering. Moreover, the geological model is mostly stationary across the entire area (except for deltaic deposits), and channel deposits account for a high proportion. Therefore, whether well locations are selected manually or randomly, the representativeness of the 4-well dataset shows little difference. Training samples from both channel and non-channel facies can be obtained (Fig. 4). These wells, when paired with seismic data at varying frequencies (e.g., 20 Hz, 30 Hz, 40 Hz, 50 Hz, and 60 Hz), form a comprehensive training dataset for deep learning models. This experimental design allows for a comprehensive assessment of the robustness and generalization capability of the models when trained on datasets of different sizes. The subsequent analyses will begin with the moderate well condition scenario of 20 wells.

4. Results

Based on the key factors influencing seismic porosity inversion, we conducted a series of inversion experiments to systematically evaluate the impacts of seismic spectral decomposition, Bayesian inversion methods, seismic resolution, and well quantity on inversion performance.

4.1. Impact of seismic spectral decomposition on porosity inversion

Seismic data preprocessing and feature extraction play a crucial role in enhancing the performance of deep learning models. Spectral decomposition techniques enhance seismic porosity inversion by transforming seismic data from the time domain to the frequency domain, thereby revealing the responses of reservoir characteristics across different frequency bands. Seismic data at different frequencies exhibit varying sensitivities to reservoir thickness. This method improves the accuracy and reliability of porosity prediction by highlighting frequency components closely related to reservoir thickness and porosity, while reducing the influence of noise and tuning effects.

To evaluate the impact of spectral decomposition on porosity prediction, we tested the performance of both the WaveNet and SpecNet models (Table 1) under Scenario 2 (moderate well condition, Table 2). WaveNet processes input seismic waveforms in the time domain, whereas SpecNet operates on spectra in the time-frequency domain. These models were trained using 20 wells and the 40 Hz seismic data. Their performance was tested across the entire 3D volume, totally 30,000 traces, to assess generalization capability and spatial consistency of porosity predictions.

Fig. 6 displays the input seismic data and the corresponding true porosity distribution. Fig. 7 presents the porosity prediction results generated by the WaveNet and SpecNet models. The SpecNet model achieves a mean absolute error (MAE) of 0.0480 on the full 3D test volume, outperforming the WaveNet model. From the map view, the porosity predictions generated by SpecNet exhibit improved spatial continuity of the meandering channel structures. From the cross-sectional perspective, the prediction performance of thick-channel sand bodies is comparable between the two methods. SpecNet performs better in predicting thin-layer meandering channel and deltaic sand bodies than WaveNet.

4.2. Bayesian vs. non-Bayesian models for porosity inversion

We evaluated two Bayesian models, BayeWaveNet and BayeSpecNet, which integrate WaveNet and SpecNet architectures with Bayesian deep learning frameworks (see Table 1). Under Data Scenario 2 (moderate well condition, Table 2), all models were trained using 20 wells and the 40 Hz seismic data. Their performance was assessed on the entire 3D volume to quantify predictive accuracy and uncertainty estimation capability.

Bayesian models, BayeWaveNet and BayeSpecNet, employ Monte Carlo dropout to perform multiple stochastic predictions during inference. Fig. 8 shows that, as the number of stochastic forward passes increases, the prediction error of Bayesian deep learning model decreases significantly. Since Bayesian deep learning introduces stochasticity in network weights, the prediction results exhibit large randomness when only a single prediction or a small number of predictions are performed, leading to relatively large errors from the ground truth. As the number of predictions increases, the averaged prediction results and the estimated standard deviation become more stable. However, the non-Bayesian models, WaveNet and SpecNet, maintain consistent predictions regardless of the number of stochastic realizations (Fig. 8), as their deterministic nature does not incorporate variational inference or probabilistic sampling. For both BayeWaveNet and BayeSpecNet, the prediction error stabilizes after 15 Monte Carlo realizations, with no significant further reduction observed beyond this point (Fig. 8). Therefore, for Bayesian inference, we selected 15 prediction realizations to serve as the Monte Carlo sampling frequency, which balances computational efficiency and the stability of the prediction and uncertainty estimates.

When deploying the trained Bayesian deep learning model on the 3D data volume, for each spatial point in the 3D volume, we first perform 15 rounds of stochastic forward propagation. The arithmetic mean and standard deviation of the 15 prediction results are taken as the final porosity prediction and the corresponding quantitative uncertainty estimate, respectively. In this way, the final 3D porosity volume and the corresponding uncertainty volume from the Bayesian deep learning prediction are obtained. Fig. 9 shows the slices of the porosity prediction and associated uncertainty volumes obtained from the Bayesian models.

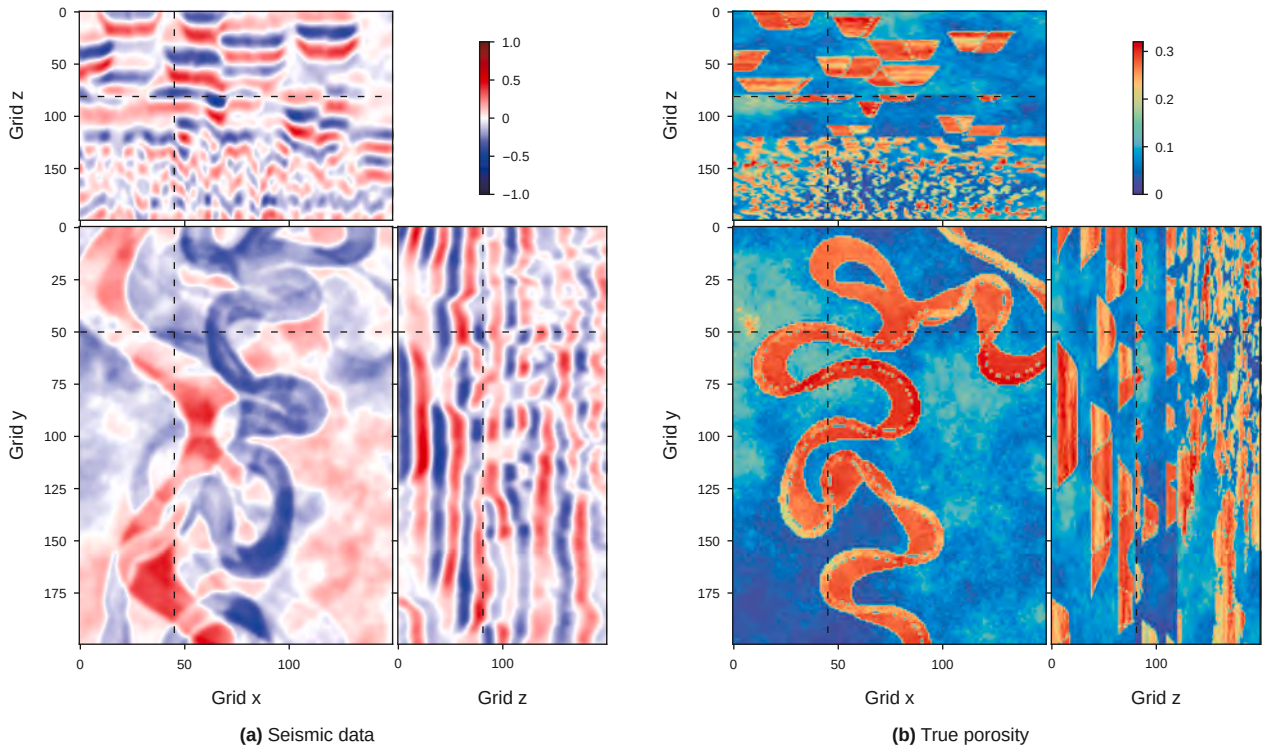


Fig. 6. Slice visualizations of seismic data and porosity data for model training. The sub-figures display three slices along the *x*, *y*, and *z* directions within the 3D volume. The positions of these slices are plotted by dashed lines. **(a)** Slices of the 3D seismic data of 40 Hz. **(b)** Slices of the 3D true porosity data.

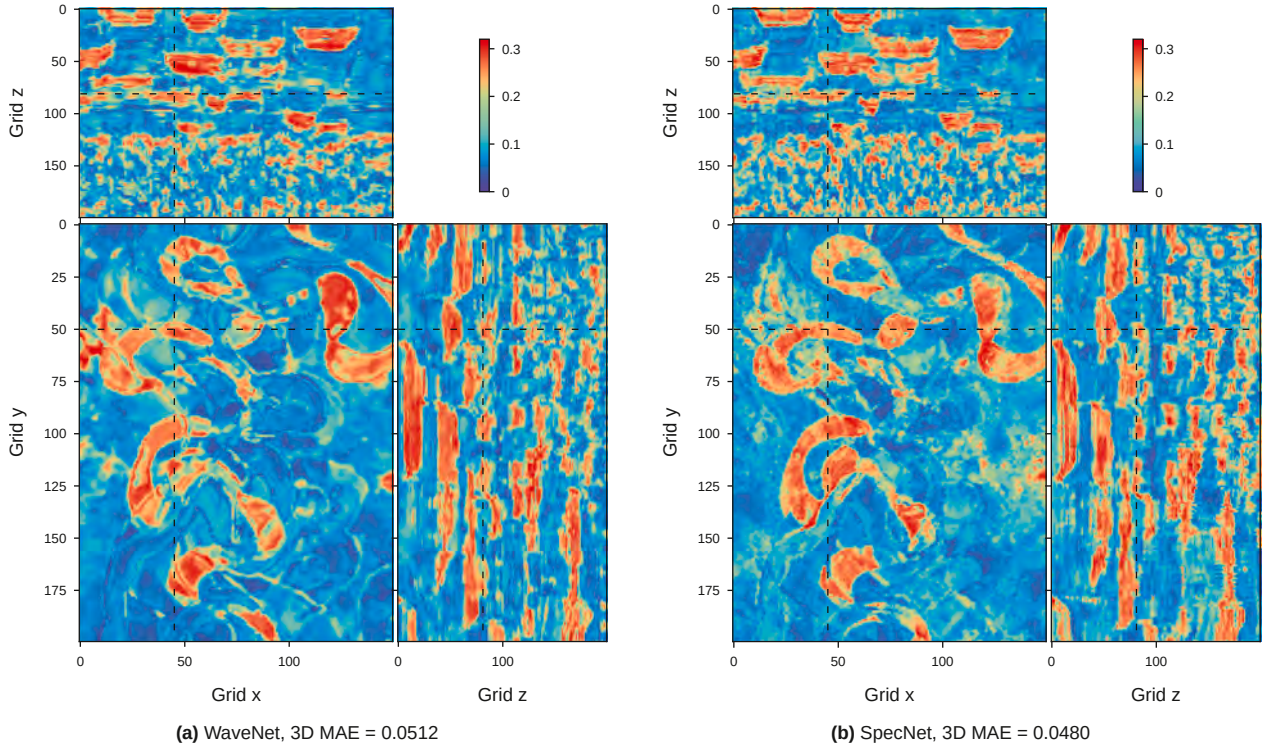


Fig. 7. Porosity prediction results of WaveNet and SpecNet models. **(a)** WaveNet prediction slices (3D MAE = 0.0512). **(b)** SpecNet prediction slices (3D MAE = 0.0480). Each subfigure illustrates three orthogonal slices extracted from the 3D volume along the *x*-, *y*-, and *z*-directions. The locations of these slices are indicated by dashed lines.

Fig. 9a and b presents the porosity estimation results obtained from the Bayesian BayeWaveNet and BayeSpecNet models. These models achieve mean absolute errors (MAE) of 0.0472 and 0.0448, respectively, on the full 3D test volume, outperforming their non-Bayesian counterparts (WaveNet and SpecNet) shown in Fig. 7. The porosity predictions generated by the Bayesian models exhibit

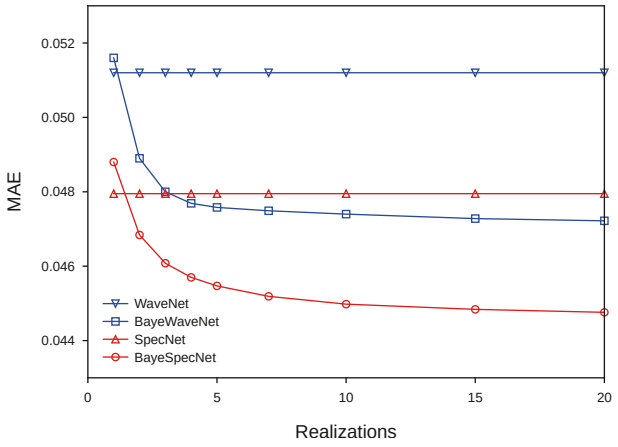


Fig. 8. MAE curves of WaveNet, B-WaveNet, SpecNet, and B-SpecNet with different realizations.

reduced noise and greater geological coherence. In map view, the Bayesian approaches also demonstrate enhanced spatial continuity in meandering channel structures compared to the non-Bayesian results in Fig. 7. Among all these four evaluated methods, BayeSpecNet achieves the best overall performance in terms of prediction accuracy and spatial continuity.

Fig. 9c and d presents the uncertainty estimation results obtained from the Bayesian BayeWaveNet and BayeSpecNet models. As shown in the figure, regions with warmer (redder) colors indicate higher predictive uncertainty. Specifically, thin sand bodies exhibit greater uncertainty compared to thick sand bodies, while the edges of thick sand bodies show higher uncertainty than their central parts. In the porosity prediction results, areas where channels are discontinuous are associated with elevated higher uncertainty. This implies that certain realizations of the Bayesian models are capable of predicting discontinuous channel segments. These patterns help improve our understanding of channel connectivity and support the geologic interpretation of spatial continuity.

Fig. 10 shows average MAE distribution binned by uncertainty for both BayeWaveNet and BayeSpecNet models. We divide the uncertainty estimates into 5 bins according to their values (0-0.02, 0.02-0.04, 0.04-0.06, 0.06-0.08, 0.08-1.00), and calculate the average MAE of each bin. The results show that the average MAE increases significantly with the increase of uncertainty bin. This monotonic increase in MAE with increasing uncertainty confirms that the standard deviation-based uncertainty estimates are well-calibrated and effectively reflect the reliability of model predictions. Moreover, across all uncertainty intervals, BayeSpecNet consistently yields a slightly lower average MAE compared to BayeWaveNet, indicating a stable advantage in predictive accuracy.

4.3. Impact of well quantity on seismic porosity inversion

Deep learning models trained on well logs and adjacent seismic data represent one of the most widely used data-driven methods in practical applications. The number of available wells significantly influences the generalization capability and prediction accuracy. To systematically evaluate this effect, we designed multiple training scenarios with varying well quantities and assessed the performance of different models under these conditions.

We first focus on BayeSpecNet, the best-performing model identified in the previous section, and examine its performance across three training data scenarios: 4, 20, and 266 wells, all using the 40 Hz seismic data (Table 2). The amount of well data used for model training has a direct impact on prediction accuracy and uncertainty estimation.

Fig. 11 compares the porosity prediction results and the associated predictive uncertainty of BayeSpecNet under different well-data training scenarios. Compared with the model trained using 20 wells (Fig. 9b), the model trained with only four wells exhibits a substantially larger prediction error in the 3D volume (Fig. 11a). The lateral continuity of channel sand bodies in plan view is noticeably degraded, while the geometry and connectivity of channel sand bodies in cross-sectional views become ambiguous. In particular, the thickness of thin sand bodies is poorly resolved under sparse well control. Correspondingly, the uncertainty map (Fig. 11c) shows relatively high uncertainty values and pronounced spatial variability, especially in regions with complex channel geometry. These high-uncertainty zones are mainly distributed away from well control and within structurally complex or thin channel deposits.

In contrast, when the number of training wells increases to 266 (Fig. 11b), the porosity predictions become significantly more coherent and geologically consistent. The meandering channel architecture is clearly delineated, with improved lateral continuity and reduced background noise. In cross-sectional views, the geometry and connectivity of channel sand bodies are much better resolved, and the thickness of thin sand bodies is predicted more accurately. This improvement is further reflected in the uncertainty estimates (Fig. 11d), where both the magnitude and spatial extent of high-uncertainty regions are markedly reduced. Lower uncertainty values are observed within well-constrained channel bodies, whereas relatively higher uncertainty remains mainly in structurally complex or thin channel zones.

Overall, the comparison demonstrates that increasing well density not only improves the accuracy of porosity prediction, as indicated by the reduced 3D MAE, but also leads to a more reliable and spatially consistent uncertainty quantification. These results further suggest that limited well data reduce the representativeness of the training samples, thereby increasing epistemic uncertainty in the predictions, while a larger number of training wells improves sample representativeness and correspondingly reduces predictive uncertainty.

4.4. Impact of seismic frequency on seismic inversion

We also investigate the porosity prediction performance of the deep learning model under seismic data with different frequency. Specifically, we first examine the performance of the BayeSpecNet model across three seismic data scenarios with dominant frequencies of 20, 40, and 60 Hz, all trained using 20 wells (Table 2).

Fig. 12 illustrates the effect of seismic resolution on porosity prediction and uncertainty estimation using the BayeSpecNet model. Compared with the model trained using seismic data with frequency of 40 Hz (Fig. 9b), when low-resolution seismic data with a dominant frequency of 20 Hz are used for training (Fig. 12a), the predicted porosity distribution captures the large-scale pattern of thick sands in the cross-sectional view, but fails to resolve thin meandering channels in both plan-view and cross-sectional slices. Thin meandering channel deposits appear blurred or discontinuous, and their thickness is systematically underestimated. This limitation is reflected in the corresponding uncertainty map (Fig. 12c), which exhibits relatively high uncertainty values and strong spatial variability, particularly within predicted sand zones.

In contrast, when higher-resolution seismic data with a dominant frequency of 60 Hz are employed (Fig. 12b), the porosity

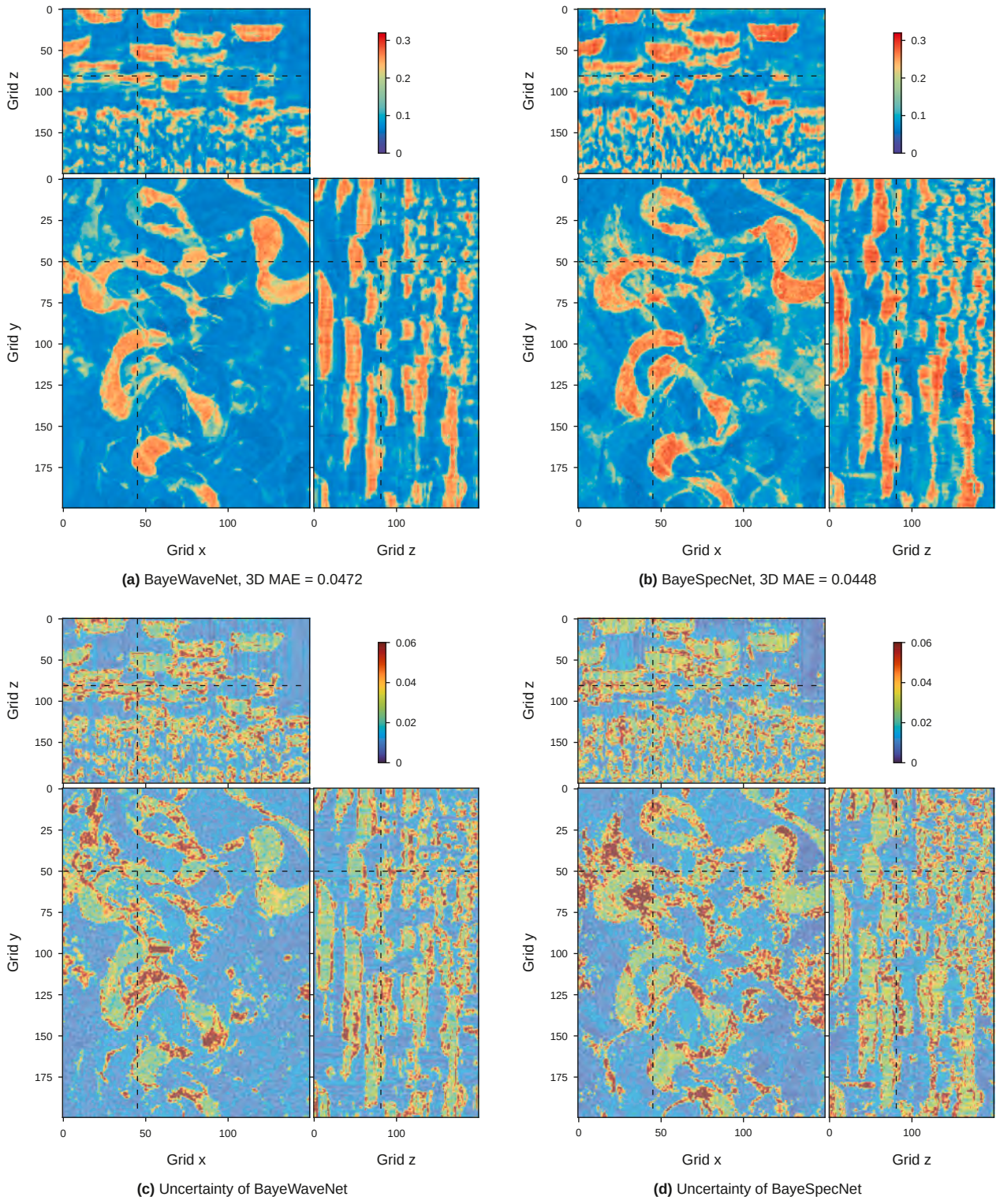


Fig. 9. Porosity predictions and associated uncertainty obtained from the BayeWaveNet and BayeSpecNet models. Panel **(a)** shows porosity prediction slices generated by BayeWaveNet (3D MAE = 0.0472), while panel **(b)** presents the corresponding prediction slices from BayeSpecNet (3D MAE = 0.0448). Panels **(c)** and **(d)** display the uncertainty prediction slices from BayeWaveNet and BayeSpecNet, respectively. Each subfigure illustrates three orthogonal slices extracted from the 3D volume along the *x*-, *y*-, and *z*-directions. The locations of these slices are indicated by dashed lines.

predictions show markedly improved delineation of channel geometry and internal heterogeneity. Thin sand bodies are more clearly resolved, with enhanced lateral continuity and more accurate thickness representation. Correspondingly, the uncertainty estimates (Fig. 12d) display a notable reduction in both magnitude and spatial extent of high-uncertainty regions. Higher uncertainty remains concentrated in areas with thinner sands or complex sand structures.

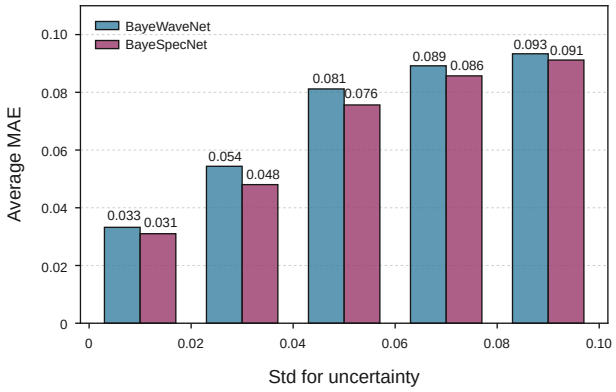


Fig. 10. MAE distribution binned by uncertainty. Uncertainty estimates (derived from standard deviation) are divided into 5 bins according to their values (0-0.02, 0.02-0.04, 0.04-0.06, 0.06-0.08, 0.08-1.00), and the average MAEs of BayeWaveNet and BayeSpecNet model predictions are calculated for each bin.

Overall, these results demonstrate that seismic resolution plays a critical role in controlling both prediction accuracy and uncertainty quantification. Low-resolution seismic data limit the model's ability to characterize thin reservoirs and lead to increased predictive uncertainty, whereas higher-resolution seismic data significantly enhance the reliability of porosity prediction and reduce uncertainty, particularly for thin channel deposits.

4.5. Influence on different sedimentary deposits

Different depositional facies are characterized by distinct sand thicknesses and spatial architectures, which lead to varying levels of prediction difficulty. The uppermost sinuous channel facies is composed of relatively wide and thick sands, resulting in the strongest seismic expression and, consequently, the lowest prediction difficulty. In contrast, the middle meandering channel facies exhibits higher sinuosity and thinner sands, making it more challenging to predict accurately. The lowermost deltaic facies shows strong lateral heterogeneity: in the upstream region, sands are relatively wide and thick and thus easier to predict, whereas in the downstream region, sands become narrower, more dispersed, and thinner, leading to the highest prediction uncertainty.

In the previous sections, the evaluation of model performance focused primarily on cross-sections and plan-view predictions of meandering channel systems. In this section, we further examine and compare the plan-view porosity prediction performance for sinuous channel and deltaic facies, with particular emphasis on the differences in prediction behavior associated with their contrasting depositional architectures.

Fig. 13 illustrates the effects of input representation, Bayesian inference, well density, and seismic resolution on porosity prediction for relatively thick sinuous channel deposits. Compared with the waveform-based WaveNet and BayeWaveNet (Fig. 13b and d), the time–frequency spectrum–based SpecNet and BayeSpecNet (Fig. 13c and e) produces relatively more continuous and better-defined channel geometries. However, this improvement is less pronounced than that observed for the thinner meandering channel deposits presented earlier. The predicted channels exhibit enhanced continuity in some regions but appear less continuous in others. This is mainly because the sinuous channels are relatively thick, so the high-frequency components of the time–frequency spectrum, which are sensitive to thin layers, can hardly play an effective role. Bayesian implementations further enhance prediction stability and geological consistency. Relative to their deterministic counterparts (Fig. 13b and c), Bayesian models produce predictions with noticeably less noise and greater stability (Fig. 13d and e). The influence of well density is evident when comparing BayeSpecNet results trained with 4, 20, and 266 wells (Fig. 13e–g). Sparse well control leads to fragmented channels (Fig. 13f), whereas dense well sampling substantially improves channel continuity and thickness prediction (Fig. 13h). Seismic resolution also plays a key role: low-frequency data result in blurred channel boundaries (Fig. 13h), while higher-frequency data better preserve channel edges and internal variability (Fig. 13i). The 20 Hz seismic data yield better prediction results for thick sinuous channel bodies compared with thinner meandering channel deposits (Fig. 12a). Overall, the results demonstrate that combining spectral-domain inputs, Bayesian learning, sufficient well control, and higher-resolution seismic data yields the most reliable porosity predictions for thick channel deposits.

Fig. 14 compares porosity prediction results for deltaic deposits under different modeling and data scenarios. Owing to depositional heterogeneity, the deltaic sand bodies exhibit strong spatial variability: upstream regions are characterized by wider and thicker sand bodies that are relatively easy to predict, whereas downstream areas show dispersed, narrow, and thinly interbedded sands, posing the greatest prediction challenge. Comparing waveform- and spectrum-based inputs, SpecNet and BayeSpecNet (Fig. 14c and e) generally yields clearer prediction than WaveNet and BayeWaveNet (Fig. 14b and d), particularly in the downstream thin and fragmented delta-front deposits. Bayesian models further enhance prediction stability. Relative to their deterministic counterparts (Fig. 14b and c), Bayesian models (Fig. 14d and e) produce smoother and low-noise spatial patterns. Sparse well control (Fig. 14f) results in poorly continuous downstream sands, whereas increasing the number of wells (Fig. 14h) significantly enhances lateral continuity. Seismic resolution has a stronger impact on the prediction of downstream thin-bedded sand bodies. Low-frequency seismic data (20 Hz; Fig. 14h) limit the resolution of thin deltaic sands, while higher-frequency data (60 Hz; Fig. 14i) better capture sand-body geometry.

Overall, the results demonstrate that combining spectral-domain inputs, Bayesian learning, sufficient well control, and higher-resolution seismic data yields the most reliable porosity predictions both for thick sinuous channel deposits and complex deltaic systems.

4.6. Comprehensive analysis of multi-factor influence

This section presents a comprehensive integrated analysis of four critical factors: seismic input representation, Bayesian inference, training well density, and seismic resolution. By systematically comparing the prediction accuracy (MAE) and uncertainty across diverse scenarios, we investigate how these variables interact to influence the characterization of channel sands.

Fig. 15 quantitatively summarizes the impacts of input representation, Bayesian inference, training well density, and seismic resolution on porosity prediction accuracy and uncertainty. Overall, the models using time–frequency spectral inputs (SpecNet and BayeSpecNet) consistently outperform their waveform-based counterparts (WaveNet and BayeWaveNet), yielding lower 3D MAE across all seismic frequency scenarios (Fig. 15a). This improvement becomes more pronounced as seismic frequency decreases, indicating that spectral representations are more effective in exploiting high-resolution seismic information, particularly for resolving thin and laterally heterogeneous channel sands.

Incorporating Bayesian inference further enhances model performance and reliability. Compared with non-Bayesian models,

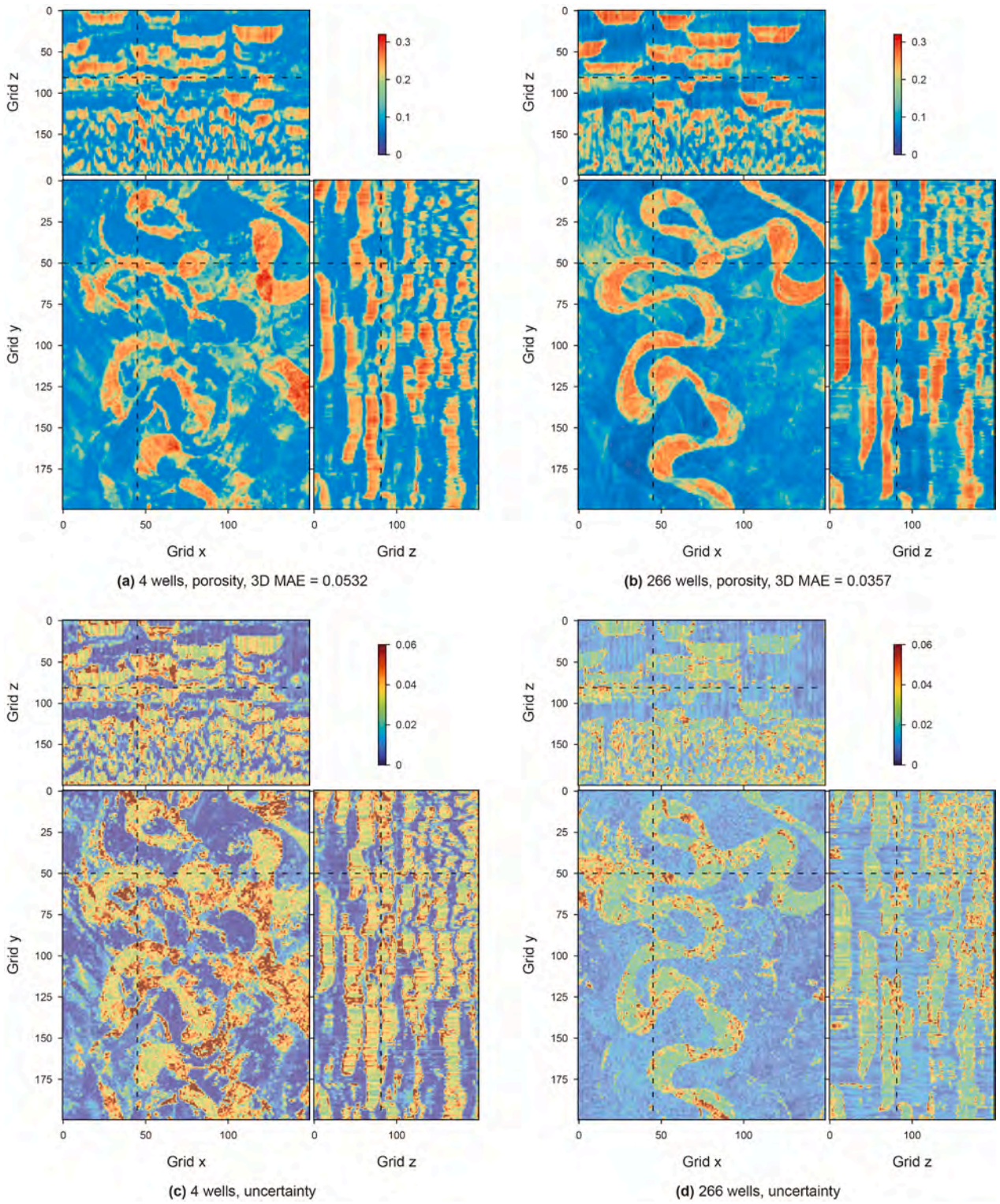


Fig. 11. Porosity predictions and associated uncertainty estimated by BayeSpecNet under different well-data training scenarios. Panels **(a)** and **(b)** show porosity prediction slices obtained using 4 and 266 wells for training, respectively, while panels **(c)** and **(d)** present the corresponding uncertainty prediction slices for the same two scenarios. Each subfigure displays three orthogonal slices extracted from the 3D volume along the *x*-, *y*-, and *z*-directions. The locations of these slices are indicated by dashed lines.

BayeWaveNet and BayeSpecNet achieve systematically lower MAE and provide stable and data-consistent estimates (Fig. 15a). The Bayesian models effectively suppress prediction noise, especially when sufficient training data are available. In contrast, non-Bayesian models exhibit higher prediction errors and lack explicit uncertainty quantification.

Training well density plays a critical role in both prediction accuracy and uncertainty. As the number of training wells increases from 4 to 266, represented by the blue, red, and black dots and lines, respectively, all models show a marked reduction in 3D MAE (Fig. 15a) and predictive uncertainty (Fig. 15b). When seismic resolution is low, increasing the number of training wells leads to a

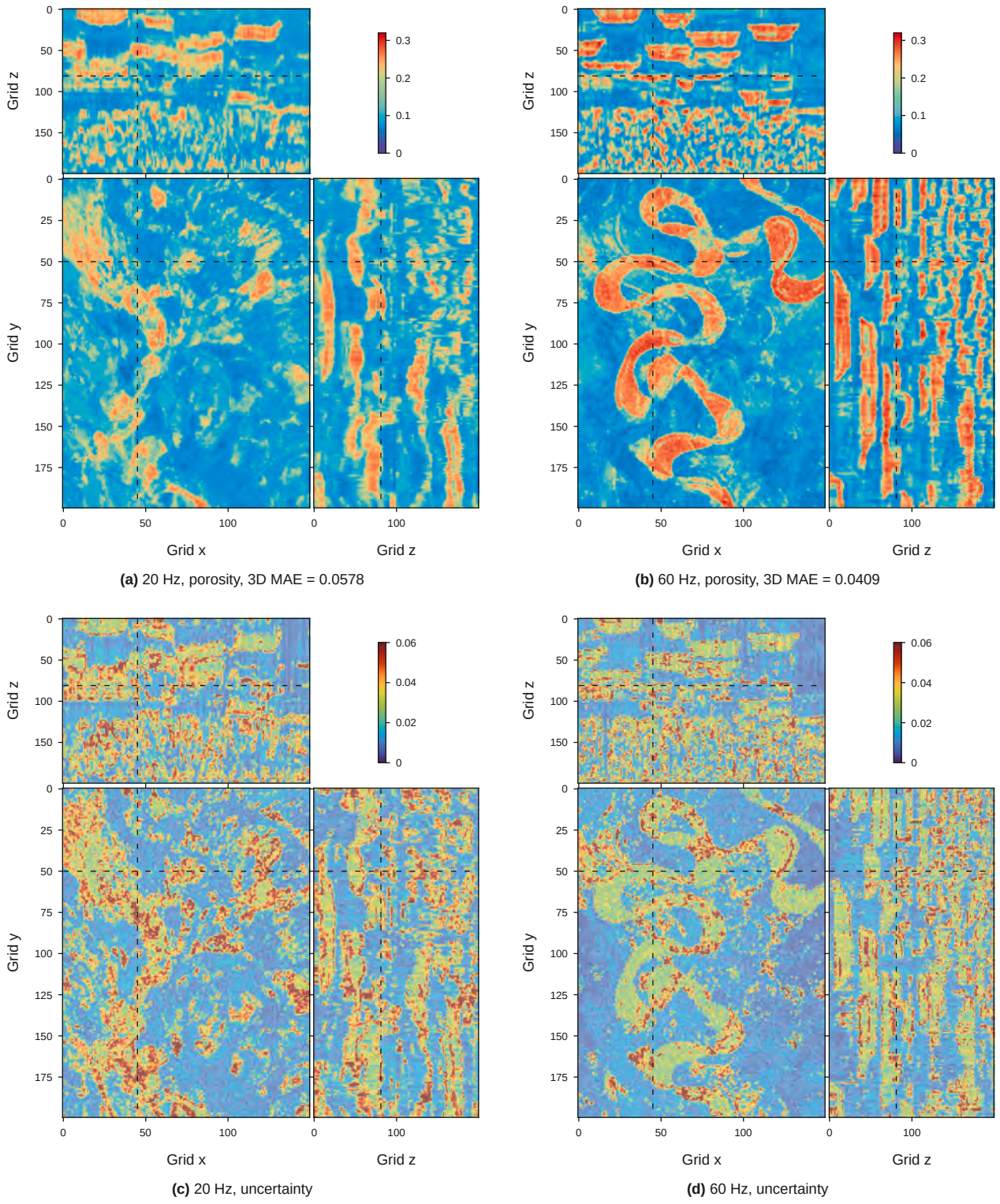


Fig. 12. Porosity predictions and associated uncertainty estimated by BayeSpecNet under different seismic frequency training scenarios. Panels **(a)** and **(b)** show porosity prediction slices obtained using 20 Hz and 60 Hz seismic data for training, respectively, while panels **(c)** and **(d)** present the corresponding uncertainty prediction slices for the same two scenarios. Each subfigure displays three orthogonal slices extracted from the 3D volume along the *x*-, *y*-, and *z*-directions. The locations of these slices are indicated by dashed lines.

more pronounced reduction in both prediction error and associated uncertainty. High well density significantly improves the representativeness of training samples, leading to more coherent porosity predictions and lower uncertainty magnitudes. Conversely, sparse well scenarios result in elevated MAE and increased uncertainty, reflecting limited data constraints and poorer generalization capability. It is noteworthy that under conditions of extremely sparse well control (e.g., 4 wells), simpler

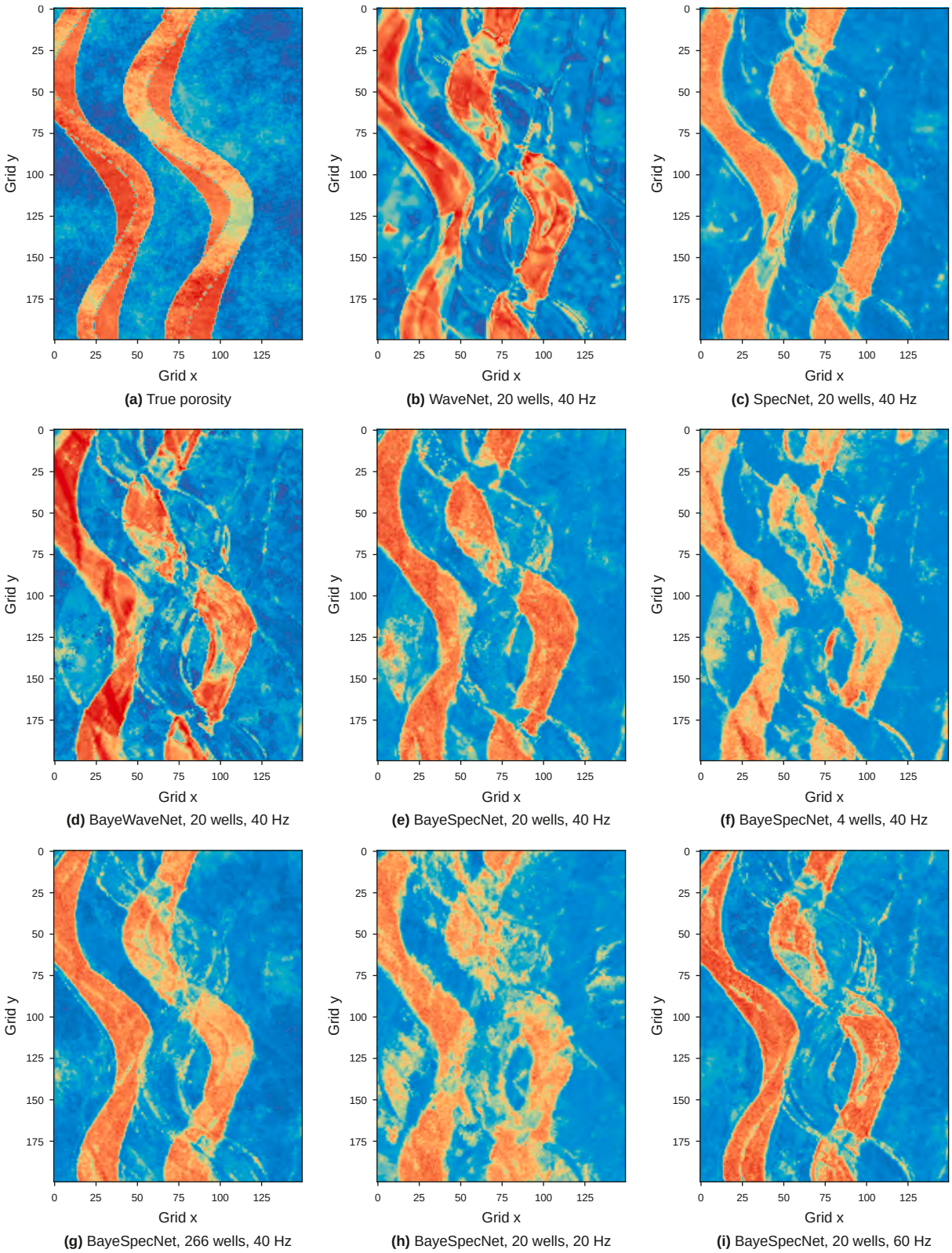


Fig. 13. Horizontal porosity prediction slices under different modeling and data scenarios for sinuous channel deposits, $z = 50$. Panel **(a)** shows the true porosity. Panels **(b)** and **(c)** present predictions from WaveNet and SpecNet trained with 20 wells and a dominant frequency of 40 Hz. Panels **(d)** and **(e)** display predictions from BayeWaveNet and BayeSpecNet under the same training conditions. Panels **(f)**–**(h)** illustrate the sensitivity of BayeSpecNet predictions to the number of wells and seismic frequency.

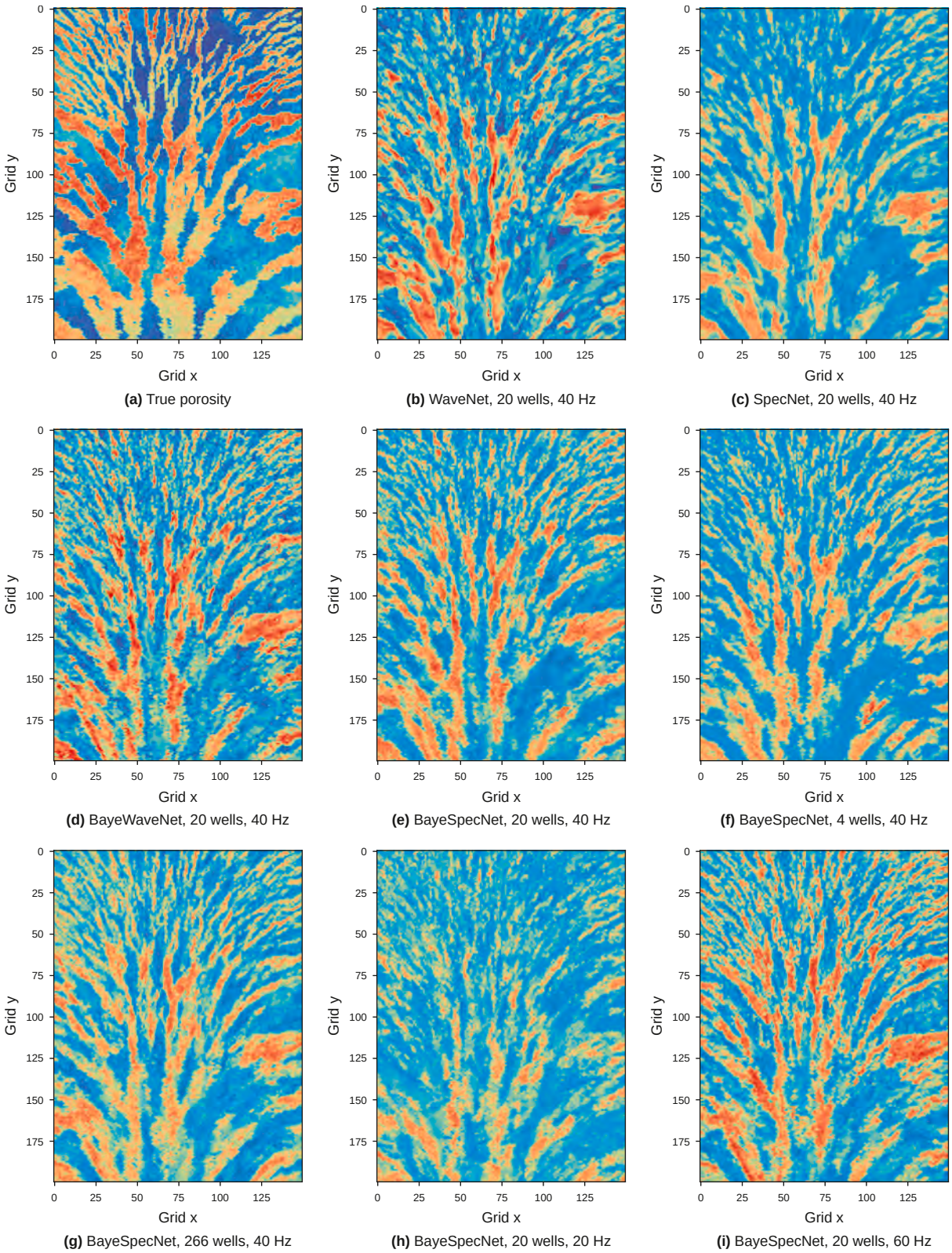


Fig. 14. Horizontal porosity prediction slices under different modeling and data scenarios for deltaic deposits, $z = 160$. Panel **(a)** shows the true porosity. Panels **(b)** and **(c)** present predictions from WaveNet and SpecNet trained with 20 wells and a dominant frequency of 40 Hz. Panels **(d)** and **(e)** display predictions from BayeWaveNet and BayeSpecNet under the same training conditions. Panels **(f)**–**(h)** illustrate the sensitivity of BayeSpecNet predictions to the number of wells and seismic frequency.

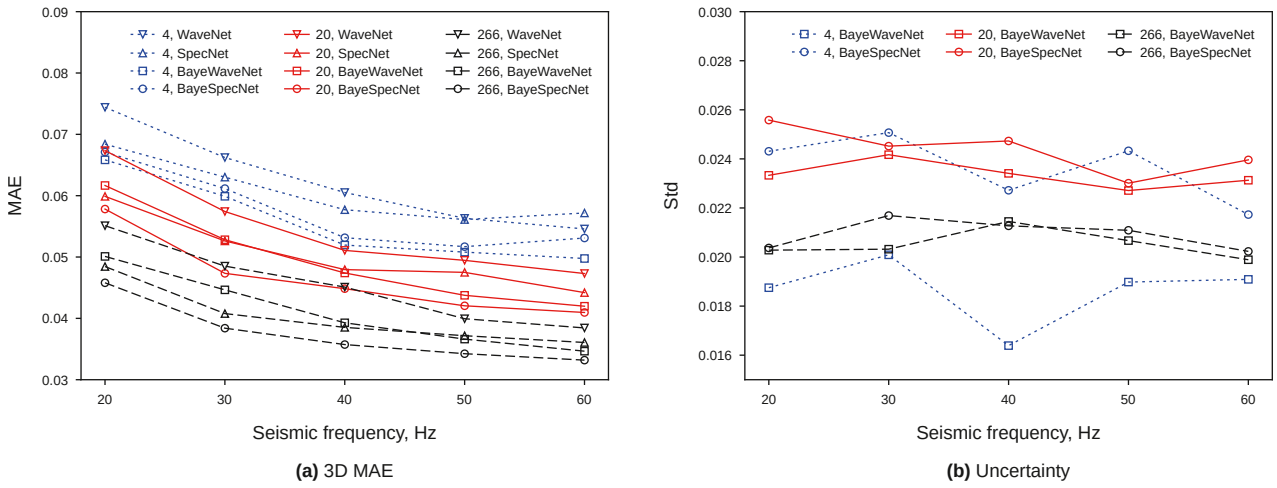


Fig. 15. Comprehensive comparison of 3D MAE and predictive uncertainty of porosity predictions for different models trained under varying training-data scenarios. Panel **(a)** shows the 3D MAE, while panel **(b)** presents the corresponding uncertainty estimates.

waveform inputs can surprisingly facilitate model convergence, leading to lower MAE and reduced uncertainty estimates (see the blue square dots and dashed lines in Fig. 15). This suggests that the inherent simplicity of waveforms may mitigate the overfitting risks when the training dataset is insufficient to constrain complex spectral features. Moreover, compared with the training scenario with more wells, limited by the quantity and representativeness of training samples, the prediction error is relatively large while the prediction uncertainty is relatively low.

Seismic resolution also exerts a clear influence on model behaviors. Increasing dominant frequency from 20 to 60 Hz leads to a consistent decrease in MAE for all models (Fig. 15a), demonstrating the importance of high-resolution seismic data for accurate porosity prediction. At the same time, predictive uncertainty tends to decrease slightly or remain stable at higher frequencies (Fig. 15b), suggesting that improved vertical resolution enhances model confidence, particularly in thin-bed settings. Notably, once seismic resolution reaches a specific threshold, its influence on prediction outcomes becomes less pronounced, as evidenced by the stabilizing MAE trends in Fig. 15a.

Overall, Fig. 15 demonstrates that the combination of spectral-domain inputs, Bayesian deep-learning frameworks, dense well control, and high-resolution seismic data yields the most accurate and reliable porosity predictions, with both reduced prediction error and physically meaningful uncertainty quantification.

5. Field example

The proposed methods were applied to porosity prediction using the field seismic data from the South China Sea, and a comparative analysis was conducted to evaluate the performance of different prediction approaches. The study area covers approximately 60 km^2, with the target formation located at a depth of around 2300 m, and six wells drilled through this interval. The target interval is characterized by marine-continental transitional clastic deposits, including deltaic distributary channels, mouth bars, and distal bars. Sandstone porosity ranges from 10% to 25%, with variable degrees of calcite cementation locally degrading reservoir quality.

The field seismic example shares key characteristics with the sparse-well synthetic training data scenario presented earlier. All six wells were calibrated to the time-domain seismic data, and each well has complete gamma ray (GR) logs and porosity logs. Five of these wells were used to train four different deep learning models, and one well (W3) was reserved as a blind test well.

Fig. 16 displays the cross-well profiles of porosity prediction results from different models. A relatively thick sand body with high porosity is developed in the middle of the target formation, showing clear seismic reflection characteristics (Fig. 16a), and all methods (including deep learning models and traditional porosity inversion based on acoustic impedance) achieve good prediction performance for this thick sand body. Thin sand bodies are developed above and below the thick sand body, respectively. The BayeSpecNet model, which integrates time-frequency input and Bayesian methods, yields the best prediction results for thin sand bodies and shows the highest consistency with the blind well W3 (indicated by the arrows in Fig. 16f). In contrast, acoustic impedance inversion and waveform-based methods exhibit poor performance in predicting thin sand bodies (Fig. 16b, c, and 16e). Fig. 17 presents the comparison of planar distribution predictions for the upper thin sand body from different methods. The BayeSpecNet model predicts a more extensive areal extent of the thin sand body, which aligns better with the observations from the blind well W3 (as indicated by the arrow in Fig. 17f).

The porosity prediction uncertainty from the BayeSpecNet model (Fig. 16h and 17h) is consistently higher than that from the BayeWaveNet model, particularly in inter-well regions. This elevated uncertainty is primarily attributed to the limited number of training wells, which constrains the representativeness of near-well seismic waveforms, and the increased complexity of learning from time-frequency spectrum inputs, which demands more data to constrain the model. Similarly, due to only the well W6 drilled with high-porosity areas is used for training, the planar prediction uncertainty is also higher in regions with higher porosity (Fig. 17g and h).

The field application results corroborate the conclusions drawn from the synthetic data experiments: the deep learning model that integrates time-frequency inputs and Bayesian inference not only improves the accuracy of thin-bed reservoir prediction but also enables a robust quantitative assessment of prediction uncertainty.

6. Discussion

This study systematically investigates how input representation, Bayesian inference, training well density, and seismic

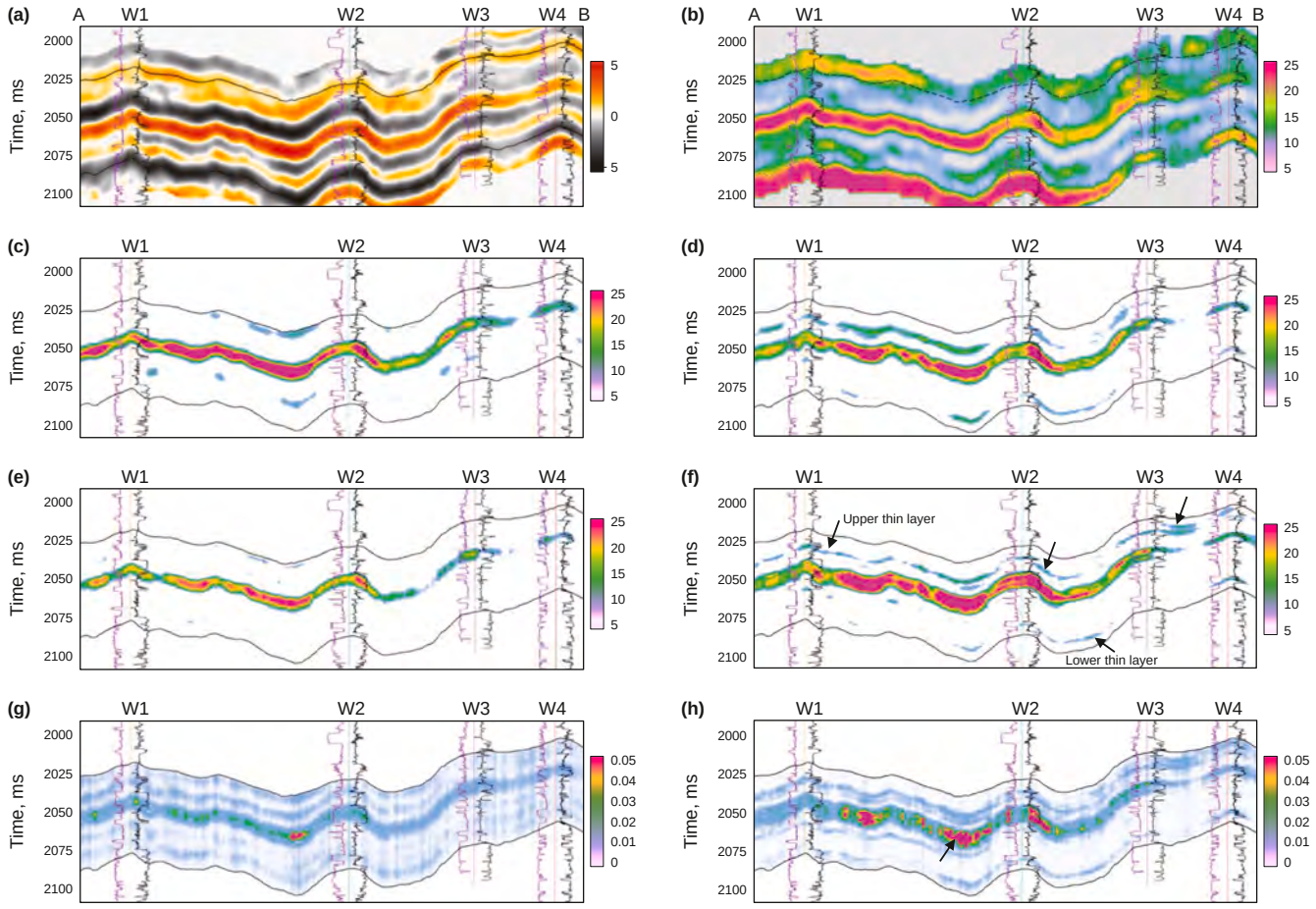


Fig. 16. Cross-well porosity prediction profiles of different deep learning models on the field seismic data. **(a)** Raw post-stack seismic profile. **(b)** Traditional deterministic porosity inversion profile based on acoustic impedance. **(c–f)** Porosity prediction results of WaveNet, SpecNet, BayeWaveNet, and BayeSpecNet models, respectively. **(g–h)** Uncertainty estimation profiles of porosity predictions from BayeWaveNet and BayeSpecNet models, respectively. The purple curve to the left of each well trajectory represents the gamma-ray (GR) log, with leftward deflection indicating lower GR values. The black curve to the right of each well trajectory represents the porosity log, with rightward deflection indicating higher porosity values. The location of this profile AB is shown in Fig. 17a.

resolution jointly influence the accuracy and reliability of deep-learning-based porosity inversion. Rather than treating these factors independently, the results reveal strong interactions among data representation, learning strategy, and data availability, which together control both prediction quality and uncertainty behavior.

Across all experimental scenarios, models using time–frequency spectral inputs (SpecNet and BayeSpecNet) consistently achieve lower 3D MAE and outperform waveform-based models. This improvement can be attributed to the ability of spectral representations to explicitly encode multiscale frequency information that is implicitly embedded but difficult to extract from raw waveforms. Seismic responses of thin beds and heterogeneous deposits are inherently frequency dependent; therefore, time–frequency spectra provide a more physically meaningful feature space for learning nonlinear relationships between seismic data and porosity. The advantage of spectral-domain inputs becomes increasingly pronounced with lower seismic resolution and in thin-bedded settings, such as meandering channels and downstream deltaic deposits. In contrast, for thick and laterally continuous sand bodies, waveform-based models already capture the dominant seismic response, resulting in relatively smaller performance differences. This observation indicates that spectral decomposition primarily enhances sensitivity to stratigraphic complexity rather than uniformly improving all depositional settings. However, caution is required when dealing with extremely sparse well data, as the increased complexity of spectral-domain inputs may predispose the model to overfitting.

Incorporating Bayesian inference through Monte Carlo dropout significantly improves both prediction stability and interpretability. Compared with deterministic models, Bayesian models produce smoother, less noisy porosity predictions and provide spatially meaningful uncertainty estimates that correlate with geological complexity, data coverage, and seismic resolution. The uncertainty maps reveal higher uncertainty in thin beds, channel margins, and areas away from well control, while thick and well-sampled sand bodies exhibit lower uncertainty. These patterns suggest that the Bayesian models effectively capture epistemic uncertainty arising from limited training data, data complexity, and non-uniqueness in the inversion process. Importantly, Bayesian inference does not merely add uncertainty outputs but also enhances predictive robustness by averaging over multiple plausible network realizations, thereby reducing sensitivity to weight perturbations.

Well density exerts a first-order control on both inversion accuracy and uncertainty magnitude. With sparse well control, the representativeness of training samples is limited, leading to fragmented channel predictions and elevated uncertainty, especially in laterally heterogeneous and thin-bedded facies. As the number

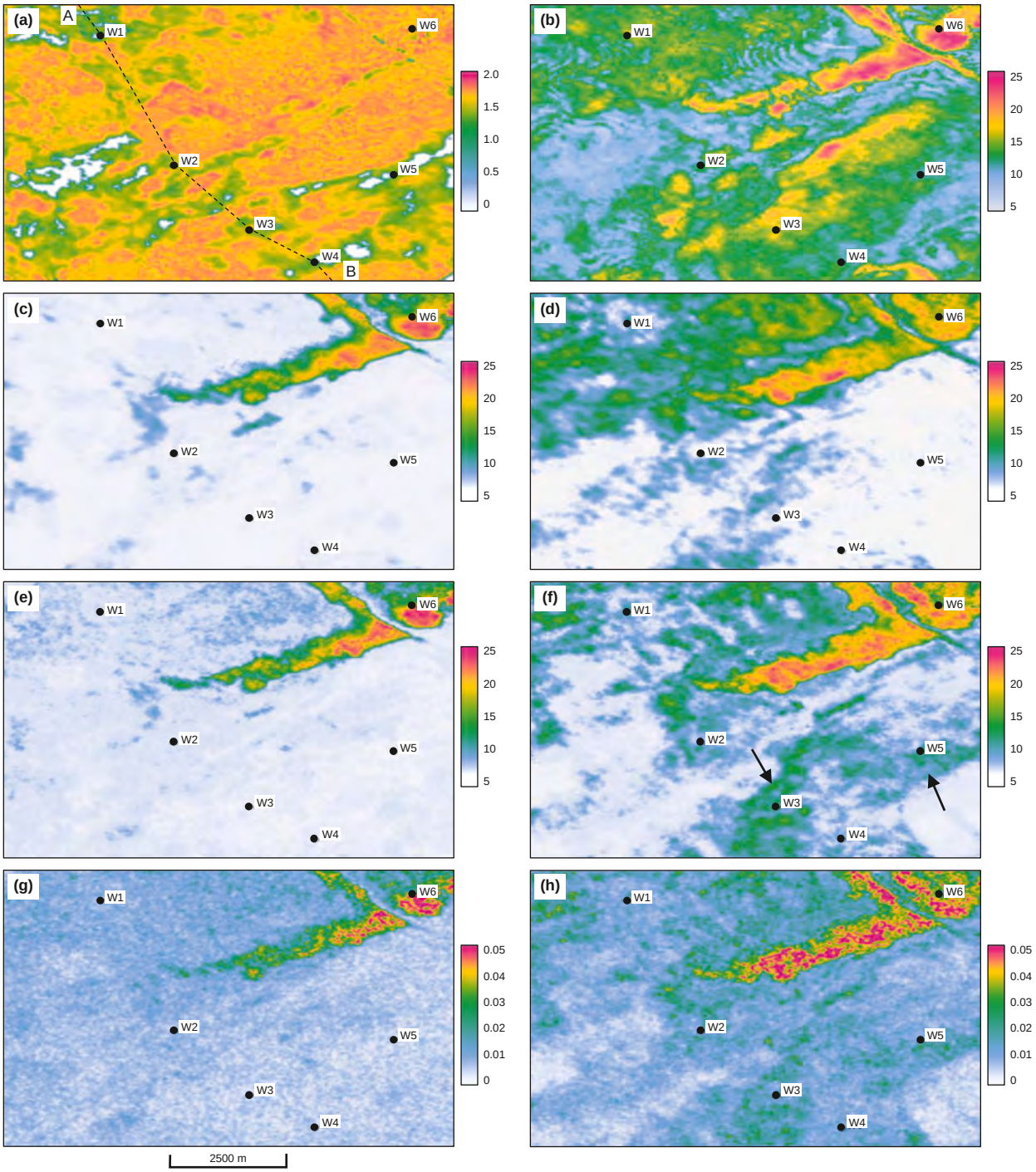


Fig. 17. Porosity prediction maps of the upper thin sand body using different deep learning models on the field seismic data. **(a)** Seismic root mean square (RMS) amplitude. **(b)** Traditional deterministic porosity inversion map based on acoustic impedance. **(c–f)** Porosity prediction maps of the WaveNet, SpecNet, BayeWaveNet, and BayeSpecNet models, respectively. **(g–h)** Uncertainty estimation maps of porosity predictions from the BayeWaveNet and BayeSpecNet models, respectively. Dashed line AB corresponds to the cross-well profile shown in Fig. 16.

of wells increases, prediction accuracy improves markedly, channel continuity becomes clearer, and uncertainty is substantially reduced. These results highlight that uncertainty estimates from Bayesian deep learning are strongly data-driven: reduced uncertainty reflects improved sample representativeness rather than model overconfidence. This behavior is particularly valuable in practical applications, where uncertainty maps can guide confidence assessment and identify regions requiring additional data acquisition.

Seismic resolution plays a critical role in constraining porosity inversion, particularly for thin and discontinuous sand bodies. Low-frequency seismic data preserve large-scale structures but fail to resolve thin layers, resulting in blurred predictions and higher uncertainty. As seismic frequency increases, both prediction accuracy and confidence improve, with the most pronounced gains observed in thin meandering channels and downstream deltaic deposits. In contrast, thick sinuous channel deposits are less sensitive to seismic resolution, as their seismic response is

already well captured at lower frequencies. This facies-dependent behavior indicates that the benefit of higher seismic resolution is not uniform but strongly controlled by depositional architecture and sand-body thickness.

Overall, the results demonstrate that the most reliable porosity inversion is achieved by combining spectral-domain inputs, Bayesian learning, sufficient well control, and adequate seismic resolution. Among all tested configurations, BayeSpecNet provides the best balance between prediction accuracy, robustness, and uncertainty quantification, particularly under realistic conditions of limited wells and band-limited seismic data. These findings suggest that Bayesian spectral-domain deep learning offers a practical and physically consistent framework for seismic inversion, enabling not only improved property prediction but also quantitative uncertainty assessment that is essential for risk-aware reservoir characterization.

Additionally, this study only focuses on several key influencing factors of seismic prediction, and tests the performance of different methods under various scenarios. However, in practical seismic prediction applications, numerous other factors are worthy of further exploration, which also constitute our future research directions. For instance, under sparse well conditions, the representativeness of well samples becomes more critical, and the impact of irregular well locations on prediction results needs in-depth investigation. Additionally, based on practical experience, seismic facies and geological trends have a significant effect on seismic prediction outcomes; thus, research on multi-trace seismic waveform constraints, seismic facies clustering, and geological trend constraints is also valuable. Furthermore, seismic data quality varies significantly across different regions and depths in practical applications, and the influence of varying seismic data quality on prediction results also deserves a thorough study.

7. Conclusion

This study systematically investigates the impacts of input representation, Bayesian inference, well data availability, and seismic resolution on porosity inversion using deep learning. Two Bayesian deep-learning frameworks, BayeWaveNet and BayeSpecNet, are proposed to jointly perform porosity prediction and uncertainty quantification.

Results from comprehensive synthetic experiments and the field example demonstrate that time–frequency spectral inputs outperform waveform-only representations, particularly for thin-bedded and laterally heterogeneous reservoirs. In cases of limited well control, the use of complex spectral features may compromise the model's generalization capability due to overfitting. Incorporating Bayesian inference further improves prediction accuracy and stability while providing physically meaningful uncertainty estimates that reflect data coverage, seismic resolution, and geological complexity.

Well density and seismic resolution are identified as two dominant factors controlling inversion performance. Sparse well scenarios and low seismic frequencies lead to degraded prediction accuracy and elevated uncertainty, especially in thin channel and deltaic deposits. In contrast, increasing well availability and seismic resolution significantly enhances both porosity prediction and uncertainty reliability. Among all tested methods, BayeSpecNet achieves the best overall performance, yielding the lowest prediction error and the most consistent uncertainty patterns across different data scenarios.

Overall, this work highlights the necessity of uncertainty-aware, spectral-domain Bayesian deep learning for seismic inversion under realistic constraints of limited wells and band-limited seismic data. The proposed framework provides a robust and practical solution for probabilistic reservoir characterization and risk-aware subsurface interpretation.

CRediT authorship contribution statement

Guo-Yin Zhang: Writing – review & editing, Writing – original draft, Visualization, Validation, Supervision, Software, Methodology, Investigation, Funding acquisition, Formal analysis, Data curation, Conceptualization. **Quan Xiong:** Writing – review & editing, Visualization, Investigation, Methodology, Validation. **Xin Zhang:** Methodology, Software. **Wen-Qi Yang:** Data curation, Visualization. **Yu-Qing He:** Investigation, Validation. **Xin-Xin Wang:** Investigation, Validation, Project administration. **Kong-Hang Yang:** Investigation, Validation. **Cheng-Yan Lin:** Funding acquisition, Project administration, Resources, Supervision.

Conflict of interest

The authors declare that there is no conflicts of interest.

Acknowledgements

The research is funded by the National Natural Science Foundation of China (Nos. 42472194, 42002144), the National Major Science and Technology Project of China (No. 2025ZD1408203-01) and the Independent Innovation Project of China University of Petroleum (No. 22CX06002A).

References

Badrinarayanan, V., Kendall, A., Cipolla, R., 2017. Segnet: a deep convolutional encoder-decoder architecture for image segmentation. IEEE Trans. Pattern Anal. Mach. Intell. 39, 2481–2495. https://doi.org/10.1109/TPAMI.2016.2644615.

Bosch, M., Mukerji, T., Gonzalez, E.F., 2010. Seismic inversion for reservoir properties combining statistical rock physics and geostatistics: a review. Geophysics 75, 75A165–75A176. https://doi.org/10.1190/1.3478209.

Castro, S., Caers, J., Mukerji, T., 2005. The Stanford Vi Reservoir: 18Th Annual Report. Stanford Center for Reservoir Forecasting. Stanford University. https://doi.org/10.1016/j.earscirev.2025.105306.

Choi, J., Kim, D., Byun, J., 2020. Uncertainty estimation in impedance inversion using Bayesian deep learning. In: SEG International Exposition and Annual Meeting. OnePetro. https://doi.org/10.1190/segam2020-3428098.1.

Das, V., Pollack, A., Wollner, U., Mukerji, T., 2019. Convolutional neural network for seismic impedance inversion. Geophysics 84, R869–R880. https://doi.org/10.1190/geo2018-0838.1.

Dong, S., Zeng, L., Du, X., Bao, M., Lyu, W., Ji, C., Hao, J., 2022. An intelligent prediction method of fractures in tight carbonate reservoirs. Petrol. Explor. Dev. 49, 1364–1376. https://doi.org/10.11698/PED.20220367.

Gal, Y., Ghahramani, Z., 2016. Dropout as a bayesian approximation: representing model uncertainty in deep learning. ICML'16 Proceedings of the 33rd International Conference on International Conference on Machine Learning 48, 1050–1059. https://doi.org/10.48550/arXiv.1506.02142.

Grana, D., Azevedo, L., De Figueiredo, L., Connolly, P., Mukerji, T., 2022. Probabilistic inversion of seismic data for reservoir petrophysical characterization: review and examples. Geophysics 87, M199–M216. https://doi.org/10.1190/geo2021-0776.1.

Kendall, A., Gal, Y., 2017. What uncertainties do we need in bayesian deep learning for computer vision. In: NIPS'17 Proceedings of the 31st International Conference on Neural Information Processing Systems, pp. 5580–5590. https://doi.org/10.48550/arXiv.1703.04977.

Kingma, D.P., Ba, J., 2014. Adam: a method for stochastic optimization. arXiv preprint arXiv:1412.6980. https://doi.org/10.48550/arXiv.1412.6980.

Lee, J., Mukerji, T., 2012. The stanford vi-e reservoir: a synthetic data set for joint seismic-em time-lapse monitoring algorithms. In: 25th Annual Report, Stanford Center for Reservoir Forecasting. Stanford University. https://pangea.stanford.edu/departments/ere/dropbox/scrf/documents/reports/25/SCRF2012_Report25/SCRF2012_15.SCRF25_Stanford20VI-E_Jaehoon2.pdf.

Li, G., Lin, C., Wu, Y., Ma, P., Tahmasebi, P., Dong, C., Liu, W., Du, X., Zhao, Z., 2025. Machine learning applications in tight porous media: challenges, advances, and future directions. Earth Sci. Rev., 105306 https://doi.org/10.1016/j.earscirev.2025.105306.

Li, P., Grana, D., Liu, M., 2024. Bayesian neural network and Bayesian physics-informed neural network via variational inference for seismic petrophysical

inversion. Geophysics 89, M185–M196. https://doi.org/10.1190/geo2023-0737.1.
Manzoor, U., Ehsan, M., Hussain, M., Bashir, Y., 2024. Improved reservoir characterization of thin beds by advanced deep learning approach. Applied Computing and Geosciences 23, 100188. https://doi.org/10.1016/j.acags.2024.100188.
Mukhopadhyay, P., Mallick, S., 2019. Bayesian deep learning for seismic facies classification and its uncertainty estimation. In: SEG Technical Program Expanded Abstracts 2019. Society of Exploration Geophysicists, pp. 2488–2492. https://doi.org/10.1190/segam2019-3216870.1.
Nair, V., Hinton, G.E., 2010. Rectified linear units improve restricted boltzmann machines. In: Proceedings of the 27th International Conference on Machine Learning. ICML-10, pp. 807–814.
Pradhan, A., Mukerji, T., 2020. Seismic bayesian evidential learning: estimation and uncertainty quantification of sub-resolution reservoir properties. Comput. Geosci. 1–20. https://doi.org/10.1007/s10596-019-09929-1.
Schaaf, A., Bond, C.E., 2019. Quantification of uncertainty in 3-d seismic interpretation: implications for deterministic and stochastic geomodeling and machine learning. Solid Earth 10, 1049–1061. https://doi.org/10.5194/se-10-1049-2019.
Song, S., Mukerji, T., Hou, J., Zhang, D., Lyu, X., 2022. Gansim-3d for conditional geomodeling: theory and field application. Water Resour. Res. 58. https://doi.org/10.31223/x5fk8b e2021WR031865.
Srivastava, N., Hinton, G., Krizhevsky, A., Sutskever, I., Salakhutdinov, R., 2014. Dropout: a simple way to prevent neural networks from overfitting. J. Mach. Learn. Res. 15, 1929–1958. https://doi.org/10.48550/arXiv.1207.0580.
Su, Z., Cao, J., Xiang, T., Fu, J., Shi, S., 2023. Seismic prediction of porosity in tight reservoirs based on transformer. Front. Earth Sci. 11, 1137645. https://doi.org/10.3389/feart.2023.1137645.
Sun, H., Zhang, J., Xue, Y., Zhao, X., 2024. Seismic inversion based on fusion neural network for the joint estimation of acoustic impedance and porosity. IEEE Trans. Geosci. Rem. Sens. 62, 1–10. https://doi.org/10.1109/TGRS.2024.3426563.
Tao, B.C., Zhou, H.L., Wu, W.Y., Zhang, G., Liu, B., Liu, X.Y., 2025. Porosity prediction based on improved structural modeling deep learning method guided by petrophysical information. Pet. Sci. 22, 2325–2338. https://doi.org/10.1016/j.petsci.2025.03.035.
Thore, P., 2015. Uncertainty in seismic inversion: what really matters? Lead. Edge 34, 1000–1004. https://doi.org/10.1190/tle34091000.1.
Xu, M., Zhao, L., Liu, J., Geng, J., 2024. Enhancing seismic porosity estimation through 3d sequence-to-sequence deep learning with data augmentation, spatial constraints, and geologic constraints. Geophysics 89, M93–M108. https://doi.org/10.1190/geo2023-0614.1.
Zeng, H., Hentz, T.F., 2004. High-frequency sequence stratigraphy from seismic sedimentology: applied to Miocene, vermilion block 50, tiger shoal area, offshore Louisiana. AAPG Bull. 88, 153–174. https://doi.org/10.1306/10060303018.
Zhang, G., Lin, C., Ren, L., Li, S., Cui, S., Wang, K., Sun, Y., 2022a. Seismic characterization of deeply buried paleocaves based on Bayesian deep learning. J. Nat. Gas Sci. Eng. 97, 104340. https://doi.org/10.1016/j.jngse.2021.104340.
Zhang, G., Wang, Z., Chen, Y., 2018. Deep learning for seismic lithology prediction. Geophys. J. Int. 215, 1368–1387. https://doi.org/10.1093/gji/ggy344.
Zhang, J., Li, J., Chen, X., Li, Y., Tang, W., 2020. A spatially coupled data-driven approach for lithology/fluid prediction. IEEE Trans. Geosci. Rem. Sens. 59, 5526–5534. https://doi.org/10.1109/TGRS.2020.3022368.
Zhang, J., Shan, X., Huo, S., Huang, L., Zheng, W., Zhou, X., Liu, E., 2025a. Deep learning-driven multi-frequency seismic inversion for enhanced thin-layer stratigraphic characterization. J. Appl. Geophys. 105749. https://doi.org/10.1109/TGRS.2020.3022368.
Zhang, J., Sun, H., Huang, X.G., Han, L., Li, Y.S., 2025b. Joint physics and model-guided pre-stack seismic inversion using double dual neural network. Pet. Sci. 23 (1), 157–177. https://doi.org/10.1016/j.petsci.2025.09.008.
Zhang, S.B., Si, H.J., Wu, X.M., Yan, S.S., 2022b. A comparison of deep learning methods for seismic impedance inversion. Pet. Sci. 19 (3), 1019–1030. https://doi.org/10.1016/j.petsci.2022.01.013.
Zhang, X., Lu, Y.H., Jin, Y., Chen, M., Zhou, B., 2024. An adaptive physicsinformed deep learning method for pore pressure prediction using seismic data. Pet. Sci. 21 (2), 885–902. https://doi.org/10.1016/j.petsci.2023.11.006.
Zhang, Y., Yang, H., 2025. Direct inversion of 3d seismic reservoir parameters based on dual learning networks. Pet. Sci. 22 (10), 4037–4051. https://doi.org/10.1016/j.petsci.2025.05.027.
Zhao, L., Meng, J., Xu, M., Wang, W., Geng, J., 2025. Seismic lithofacies prediction via deep learning with prior geological constraints. Geophysics 91 (1), MR35–MR50. https://doi.org/10.1190/geo2024-0800.
Zhao, L., Zou, C., Chen, Y., Shen, W., Wang, Y., Chen, H., Geng, J., 2021. Fluid and lithofacies prediction based on integration of well-log data and seismic inversion: a machine-learning approach. Geophysics 86, M151–M165. https://doi.org/10.1190/geo2020-0521.1.